

OPEN ACCESS

EDITED BY Bing Bai, Beijing Jiaotong University, China

REVIEWED BY
Yan Wang,
Qingdao University of Technology, China
Zhaofei Chu,
Wuhan University, China

RECEIVED 08 July 2025 ACCEPTED 30 July 2025 PUBLISHED 15 September 2025

CITATION

Song Y (2025) A new criterion for peak shear strength of rock joints based on shear-direction-related morphology description. *Front. Mater.* 12:1662066. doi: 10.3389/fmats.2025.1662066

COPYRIGHT

© 2025 Song. This is an open-access article distributed under the terms of the Creative Commons Attribution License (CC BY). The use, distribution or reproduction in other forums is permitted, provided the original author(s) and the copyright owner(s) are credited and that the original publication in this journal is cited, in accordance with accepted academic practice. No use, distribution or reproduction is permitted which does not comply with these terms.

A new criterion for peak shear strength of rock joints based on shear-direction-related morphology description

Yu Song*

Department of Civil Engineering, School of Future Cities, University of Science and Technology Beijing, Beijing, China

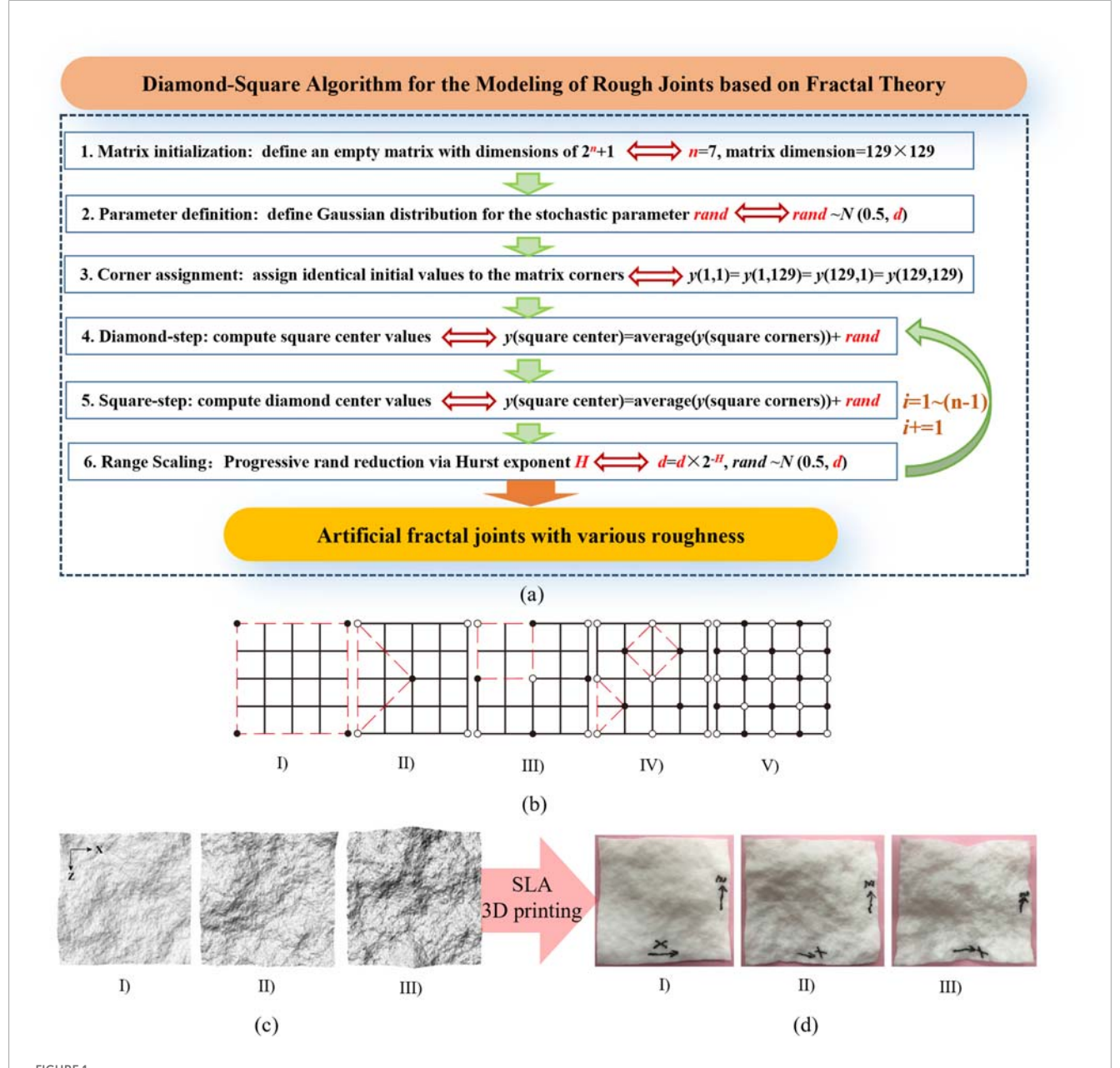
Accurate characterization of joint roughness relative to shear direction is crucial for predicting the peak shear strength (τ_p) of rough rock joints. This study proposes a modified peak shear strength criterion based on sheardirection-dependent morphological parameters. Artificial fractal joints and natural sandstone tension joints with varying roughness were replicated using 3D printing and cast in cement-based materials. Direct shear tests under constant normal load (CNL) conditions were conducted to quantify the mechanical behaviors of rough joints. Joint morphology was characterized using statistical values (mean μ , standard deviation σ) of the apparent dip angle (θ^*) distribution along the shear direction. A parameter $E(\theta^*|\theta^*>0^\circ)-\mu$, representing the conditional expectation of positive apparent dip angles relative to the shear direction, was proposed to effectively capture shear-directiondependent roughness. A new $\tau_{\scriptscriptstyle D}$ criterion incorporating this parameter was established within a Mohr-Coulomb framework. Validation against experimental data and published studies demonstrates its improved accuracy, particularly for low-roughness joints, compared to existing criteria. This approach provides a physically meaningful and efficient method for estimating τ_n , enhancing stability assessments in rock mass engineering.

KEYWORDS

joint roughness, shear direction dependency, apparent dip angle, statistical probability distribution, peak shear strength

1 Introduction

Rock joint roughness, significantly influences the shear-direction-dependent mechanical behaviors of rock joints (Hudson et al., 1997) and the hydro-mechanical characteristics within rock mass (Chang et al., 2017), further affecting the reliability of rock mass engineering. Extensive research confirms that surface morphology critically governs the shear mechanical properties of rock joints. Since the 1960s, studies incorporating morphological features of brittle materials have established diverse shear strength criteria for rough joints (Patton, 1966; Barton, 1973; Hutson and Dowding, 1987). Quantitative characterization of joint roughness is now recognized as essential for accurately evaluating shear-induced behaviors. Parameters such as Joint



Production of artificial joints models. (a) Diamond-square algorithm. (b) Midpoint displacement procedure (where, I) corner point value assignment; II) IV) Diamond steps; III) V) Square steps); (c) Artificial fractal joints with various roughness. I) A-1, d = 4 mm; II) A-2, d = 6 mm; III) A-3, d = 8 mm; (d) Solid models of artificial fractal joints. I) A-1, d = 4 mm; II) A-2, d = 6 mm; III) A-3, d = 8 mm.

Roughness Coefficient (JRC) (Barton et al., 1985), root mean square (Z_2) (Tse and Cruden, 1979; Tian et al., 2024) and fractal dimension (D) (Xie et al., 1998) are used to describe joint roughness but overlook three-dimensional (3D) joint morphology details. However, inherent non-uniformity and anisotropy complicate direction-specific roughness characterization, despite its importance for shear properties in natural rock masses (Hu et al., 2024).

Energy dissipation from particle deformation and fragmentation under shear-compression fundamentally interrelates with both dilatancy-induced shear stiffness degradation and

shear strength evolution (Bai et al., 2023; Bai et al., 2025). Consequently, quantifying morphological parameters relative to shear-direction-dependent surface detail is vital for predicting direct shear behavior. Advances in high-resolution technologies (e.g., digital image analysis, 3D scanning) enable precise digital modeling of joint surfaces (Brown, 1995; Feng and Röshoff, 2015), facilitating studies of shear-direction-dependent properties via 3D morphology (Fardin, 2008; Li et al., 2018; Ban et al., 2019). Digital Elevation Models (DEMs) derived from these techniques allow statistical quantification of 3D morphological features during shearing.

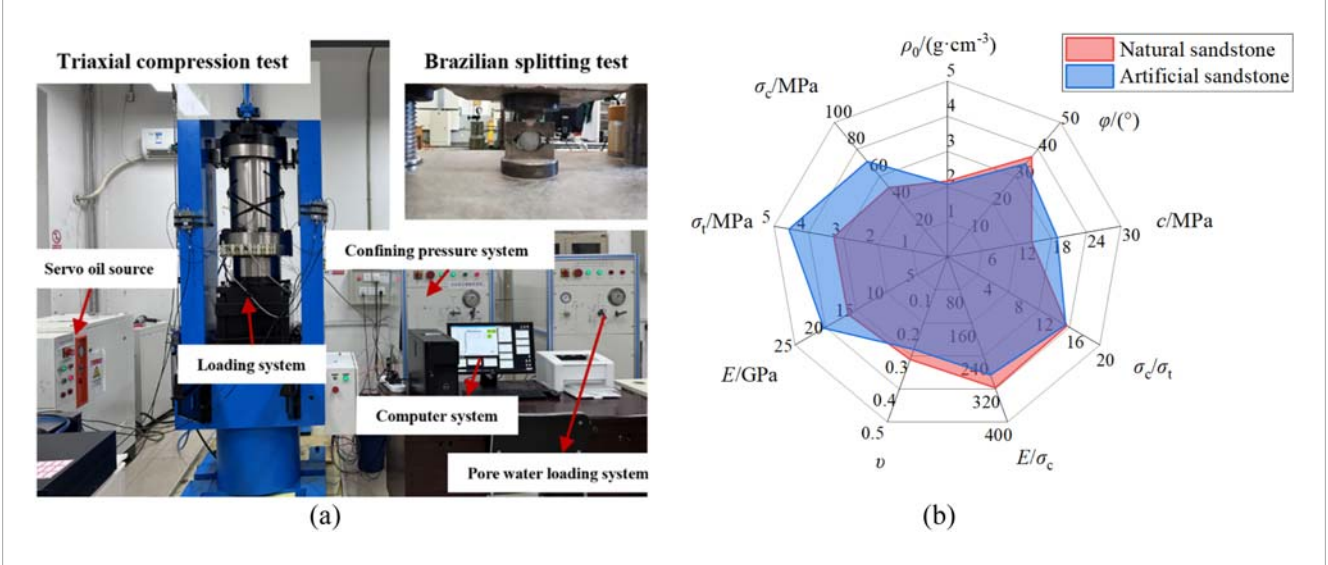
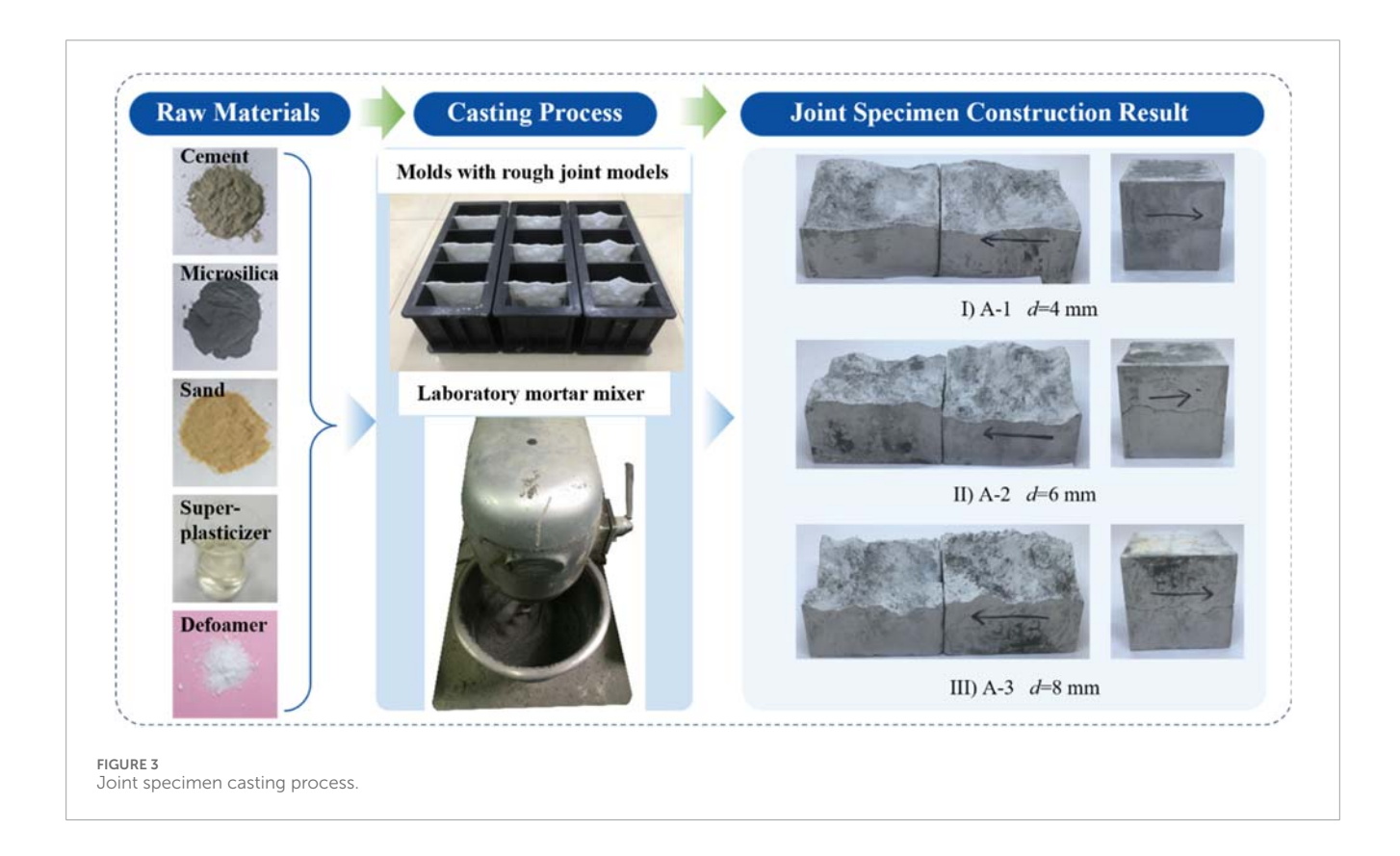
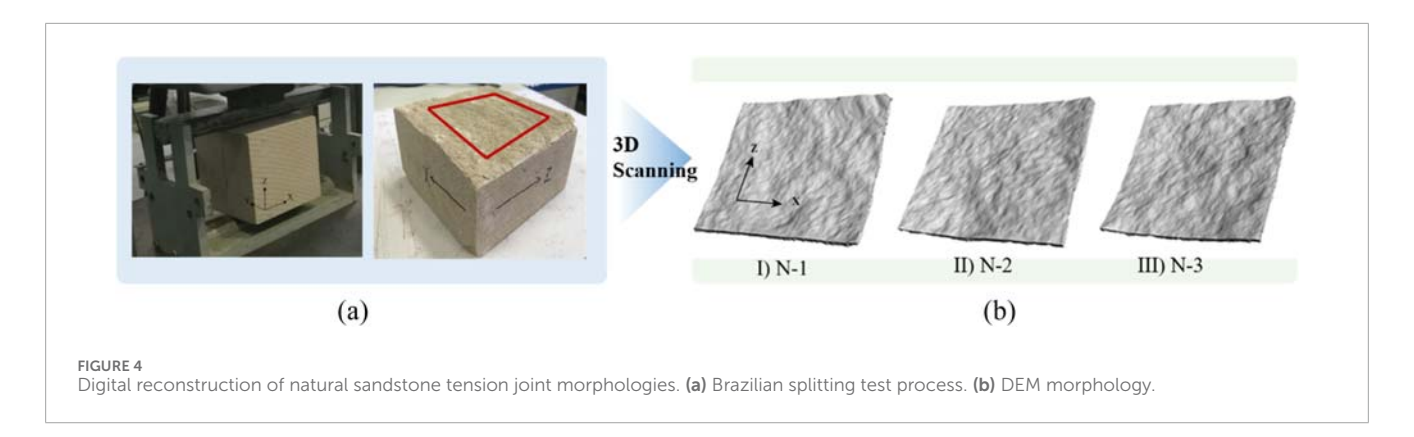


FIGURE 2
Testing on mechanical parameters of both natural and artificial sandstone. (a) Instrumentation for mechanical tests. (b) Mechanical parameters comparison.



Due to morphological anisotropy, joint roughness characterization must account for shear direction (Grasselli and Egger, 2003; Park and Song, 2013). Tian et al. (2025) summarized eight statistical morphology parameters proposed by scholars for JRC quantification. They established a new morphology-parameter-JRC dataset through inverse JRC-JCS (Joint wall compressive strength) modeling from direct shear tests, and developed a PSO-RBF (Particle swarm optimization-radial basis function) neural

network for JRC prediction. Among these parameters, Grasselli's apparent dip angle θ^* addresses joint morphological anisotropy (Grasselli and Egger, 2003), demonstrating that θ^*_{\max}/C (where θ^*_{\max} is maximum apparent dip angle, and C is a distribution parameter of θ^*) correlates with JRC under specific shear directions (Grasselli, 2006). Critically, pre-peak friction damage occurs primarily on asperities with positive θ^* values under compression, while negative- θ^* regions separate (Jiang et al., 2020). The



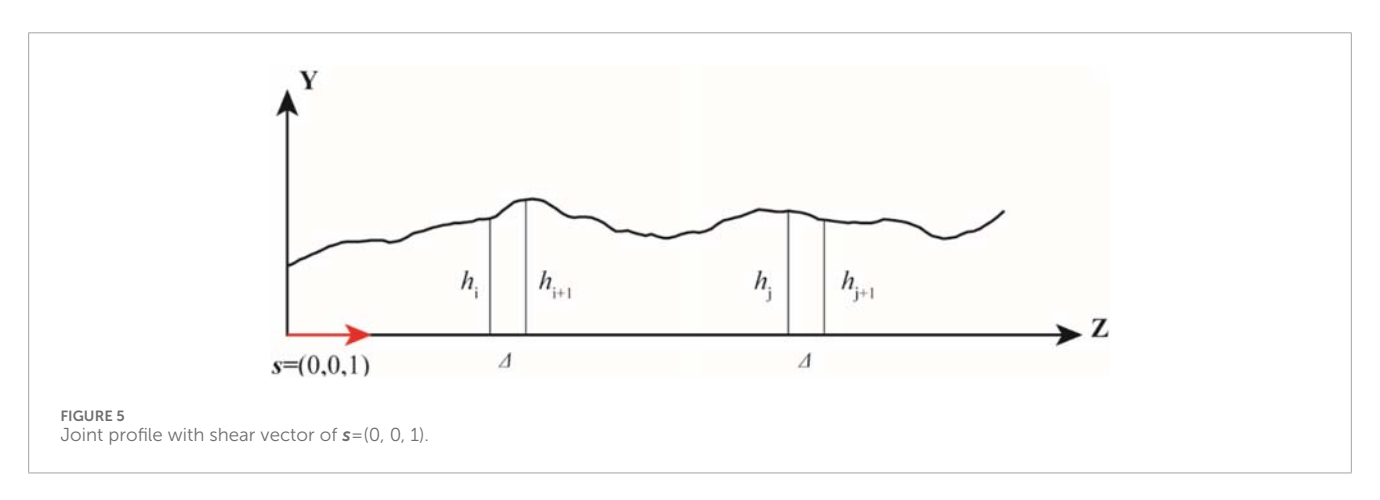


TABLE 1 JRC3D calculated by Z2.

Joint no.	N-1	N-2	N-3	A-1	A-2	A-3
JRC ^{3D}	4.13	4.68	5.45	13.09	18.94	23.45

combined role of θ^* distribution and asperity height in defining roughness is also widely accepted (Liu et al., 2017; Liu et al., 2018; Ma, Tian et al., 2020).

Quantification of shear-direction-dependent joint roughness through θ distribution is widely accepted for analyzing joint shear behavior (Tang et al., 2016; Li et al., 2017; Magsipoc et al., 2019; Li et al., 2020; Ban et al., 2021; Ríos-Bayona et al., 2021). Subsequent studies have refined Grasselli's θ -based peak shear strength criteria to better characterize joint roughness. Tatone and Grasselli (2009), Tatone and Grasselli (2014) reformulated the roughness parameter as $\theta^*_{\text{max}}/(C+1)$, incorporating sampling interval effects. Xia et al. (2014) adapted the criterion to a Mohr-Coulomb framework, characterizing morphology via dilation angle. Yang et al. (2015) integrated Barton (1973), Barton (1985) and Grasselli and Egger (2003), Grasselli (2006) theories and proposed a peak shear strength criterion in consideration of joint wall compressive strength (JCS). Tian et al. (2018) introduced resolutionindependent parameter C' to mitigate θ^-_{\max} sensitivity. Tang et al. (2021) incorporated joint wall strength difference coefficient (JSC) and developed a peak shear strength criterion for variable joint wall strengths. Ding and Li (2021) revised Xia's criterion (Xia et al., 2014) and developed a nonlinear criterion based on dilation angle evolution.

Accurate shear criteria provide a theoretical foundation for optimizing stability assessments in rock mass engineering, minimizing over-support and resource consumption while enabling durable and environmentally sustainable infrastructure. This study modifies the peak shear strength criterion using shear-direction-related morphological descriptors. Direct shear tests on joint specimens with both natural sandstone tension joints and artificial rough joints were performed. A new roughness parameter elucidating the physical meaning of $\theta^*_{\text{max}}/(C+1)$ is proposed, and a shear strength criterion compliant with the Mohr-Coulomb criterion is established and experimentally validated. This criterion shows good results in the prediction of the peak shear strength of rough joints.

2 Specimens preparation

2.1 Fabrication of artificial joints models with controlled roughness

The unevenness characterizing rock joint surface roughness exhibits continuous evolution. Therefore, methods for constructing artificial joints must accurately simulate both the 3D morphology and regional correlations of natural joints. Song et al. (2021) developed a stochastic iteration method to generate artificial fractal

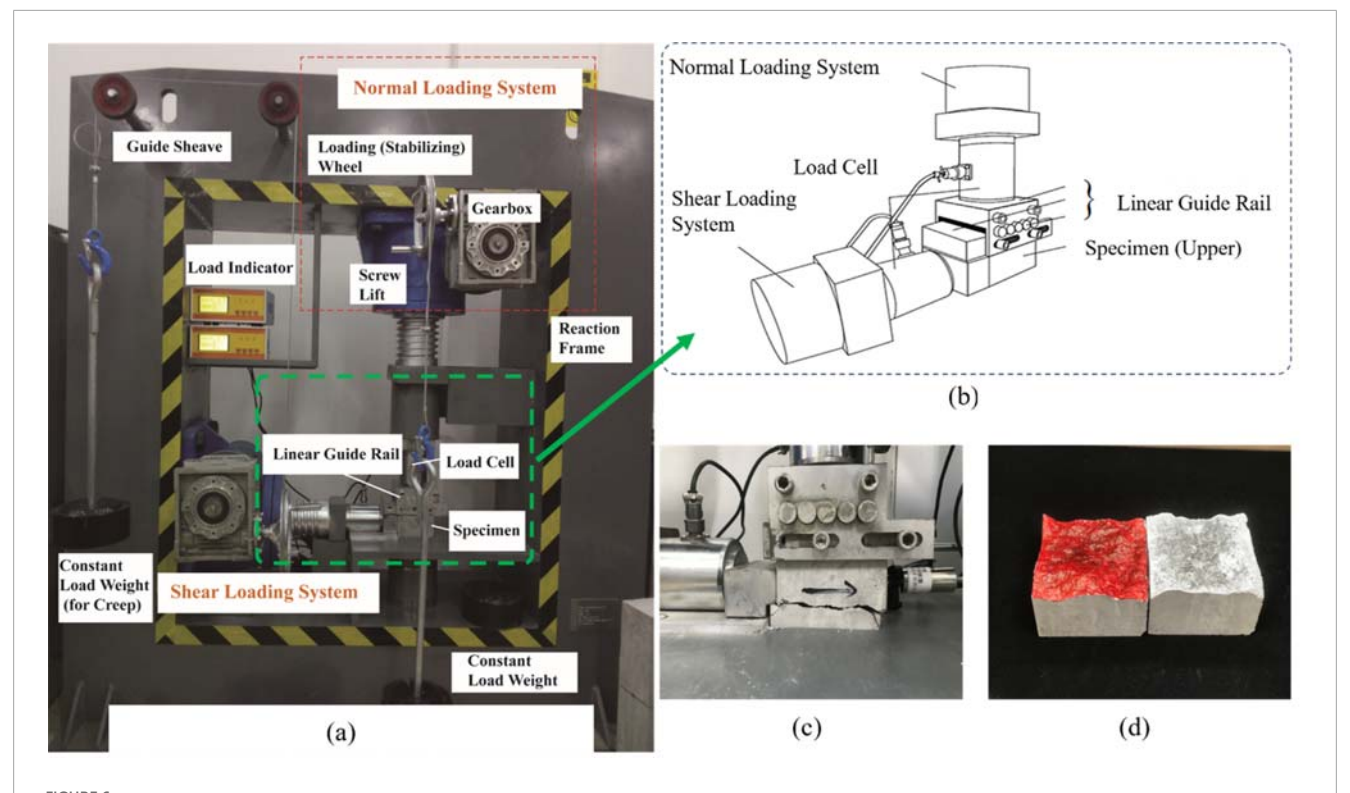


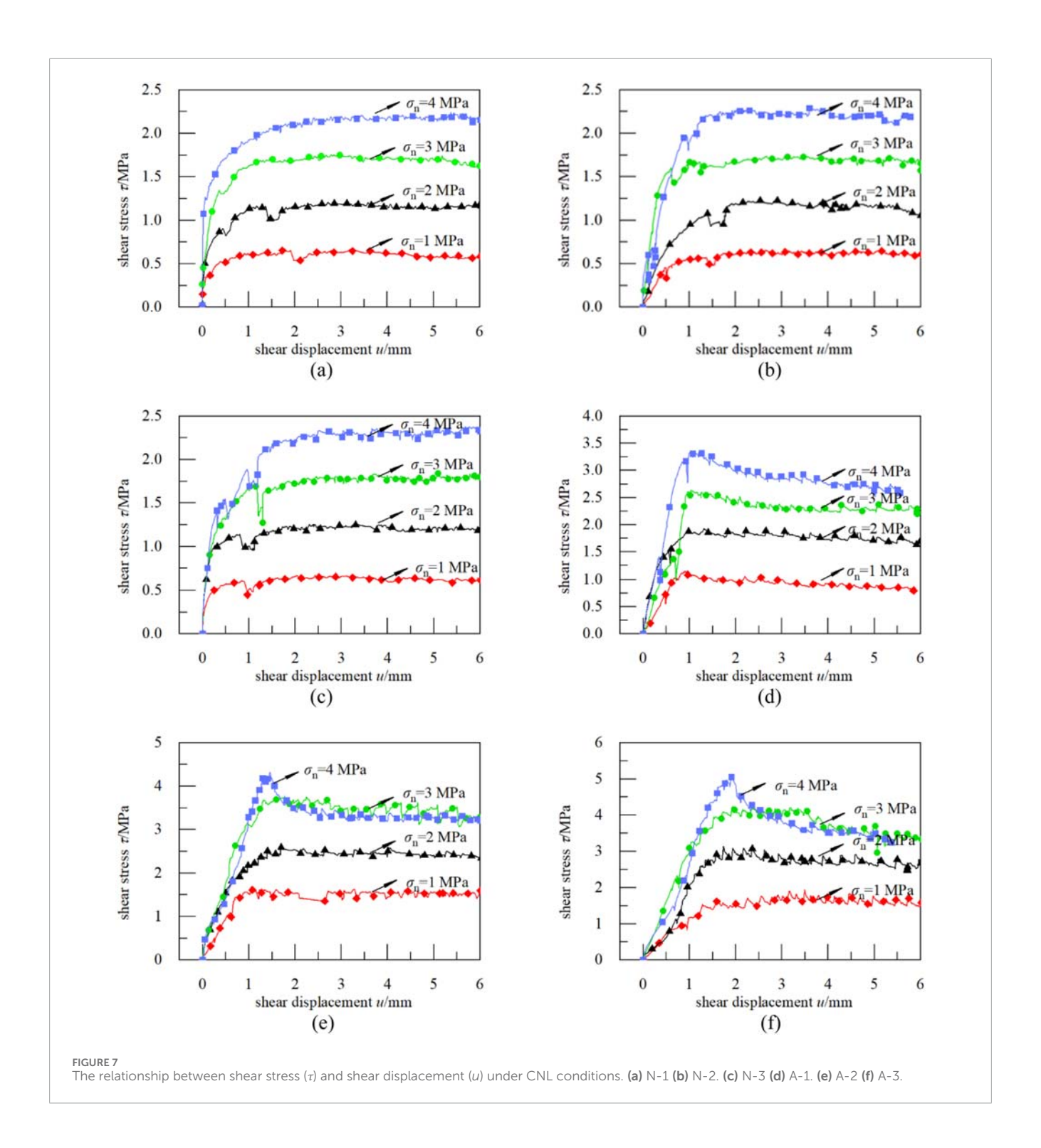
FIGURE 6
Direct shear testing implementation. (a) Gear-driven direct shearing apparatus. (b) Shear loading and displacement control of the specimen. (c) Load condition. (d) Specimen with upper part in red.

surfaces exhibiting statistical self-similarity. As shown in Figure 1a, the diamond-square algorithm was employed to populate a square grid with elevation data. In Figure 1b, black dots represent positions where new random values are generated in the current algorithmic step, while white dots indicate positions with pre-determined values from the previous step. This approach has been validated as effective for simulating rock joints with controllable roughness.

The joint surface lie within the XOZ plane, with $m = 2^n + 1$ (n = 1, 2, 3.) points uniformly distributed over the range of [-50, 50] mm along the x/z-coordinate, respectively. The elevation y at each coordinate point is determined iteratively using the diamond-square algorithm. Suppose that n = 7, the total 100 × 100 mm surface model was divided into matrix grids of 129 \times 129 with an element size $\Delta = 0.78125 \,\mathrm{mm}$; thus, the number of elements, represented by m^2 , is 16,641. Figure 1c displays the DEMs of artificial fractal surfaces generated with stochastic parameters d = 4, 6, 8 mm, denoted as model A-1, A-2, and A-3, respectively. The parameter d value determines the standard deviation of Gaussian distribution of variable rand, and further governs the 3D morphological features of the resulting fractal surfaces. It is presented that the 3D surface roughness of fractal joint surfaces increases with larger values of parameter d. Physical specimens of the digital rough joints were fabricated using additive manufacturing as Figure 1d. An OMG-450 3D printing system was applied to print the DEMs into solid specimens using ultraviolet (UV) curable resin and stereolithography appearance (SLA) technology, with 150 µm printing accuracy.

2.2 Production process of specimens with rough joints

The prototype selected in this paper is a medium-grained natural sandstone (grain size: 0.25-0.5 mm), characterized by a composition predominantly consisting of quartz (SiO₂ = 96.23%). A rock-like material replicating the deformation and brittleness of the natural prototype (Song et al., 2020) was introduced as joint wall material, where parameters E/σ_c and σ_c/σ_t were employed as quantification indices for evaluating the fidelity of the artificial sandstone. The material comprises P.O 42.5 cement and microsilica (grain size: 0.1-5 μm) as binder, and quartz sand (grain size: 0.25-0.65 mm) as aggregate. A formula of water-binder mass ratio = 0.39, sand-binder mass ratio = 0.79 and microsilica-cement mass ratio = 0.36 was selected. Laboratory tests (Figure 2a) in accordance with ISRM Suggested Methods (Eberhardt, 2009) confirmed similar physical and mechanical properties to the natural sandstone (Figure 2b). The physical and mechanical parameters of the artificial sandstone were obtained as follows: the volumetric weight $\rho_0 = 2.06 \,\mathrm{g/cm^3}$, the uniaxial compressive strength σ_c = 70.92 MPa, the Brazilian splitting strength σ_t = 4.57 MPa, the tangential modulus at 50% uniaxial compressive strength E = 20.28 GPa, the Possion's ratio v = 0.28, the cohension c =19.02 MPa, the internal friction angle $\varphi = 34.57^{\circ}$ and the basic friction angle (Alejano et al., 2018) $\varphi_b = 26.09^\circ$. Joint specimens were cast from solid models of rough joint surfaces as shown in Figure 3.



2.3 Duplication of natural sandstone tension joints

To validate the feasibility of using artificial fractal surfaces for representing joints of varying roughness, particularly for investigating the influence of joint surface morphology on sheardirection-dependent mechanical properties, specimens containing natural joints are required for comparison. Natural sandstone tension joints were produced by conducting Brazilian splitting tests on three 150 mm \times 150 mm \times 150 mm cubic sandstone blocks (natural sandstone mentioned in Section 2.2) along the z-axis. The testing process and the natural tension joint obtained are shown in Figure 4a.

A 3D Camega optical scanning system (sampling interval 25 $\mu m)$ captured point clouds of rough joints. To mitigate boundary effects, rectangular regions (100 mm \times 100 mm) from the central

TABLE 2 Shear parameters of joint specimens under various normal stresses.

Joint no.	JRC ^{3D}	$\sigma_{\sf n}/{\sf MPa}$	$ au_{ extsf{p-measured}}/ extsf{MPa}$	$ au_{ ext{r-measured}}/ ext{MPa}$	Shear strength reduction/%	
		1	0.65	0.62	4.62	
N-1	4.13	2	1.20	1.20	0.00	
N-1	4.13	3	1.75	1.68	4.00	
		4	2.23	2.19	1.79	
		1	0.66	0.66	0.00	
N-2	4.60	2	1.23	1.11	9.76	
	4.68	3	1.74	1.72	1.15	
		4	2.29	2.26	1.31	
		1	0.67	0.65	2.99	
N-3	5.45	2	1.26	1.21	3.97	
		3	1.84	1.87	-1.63	
		4	2.37	2.39	-0.84	
		1	1.14	0.86	24.56	
A-1	13.09	2	1.93	1.71	11.40	
A-1	13.09	3	2.63	2.26	14.07	
		4	3.36	2.57	23.51	
	18.94	18.94	1	1.59	1.55	2.52
A-2			2	2.60	2.45	5.77
			3	3.69	3.16	14.36
		4	4.32	3.33	22.92	
		1	1.95	1.76	9.74	
A-3	22.45	2	3.15	2.58	18.10	
A-3	23.45	3	4.24	3.32	21.70	
		4	5.05	3.31	34.46	

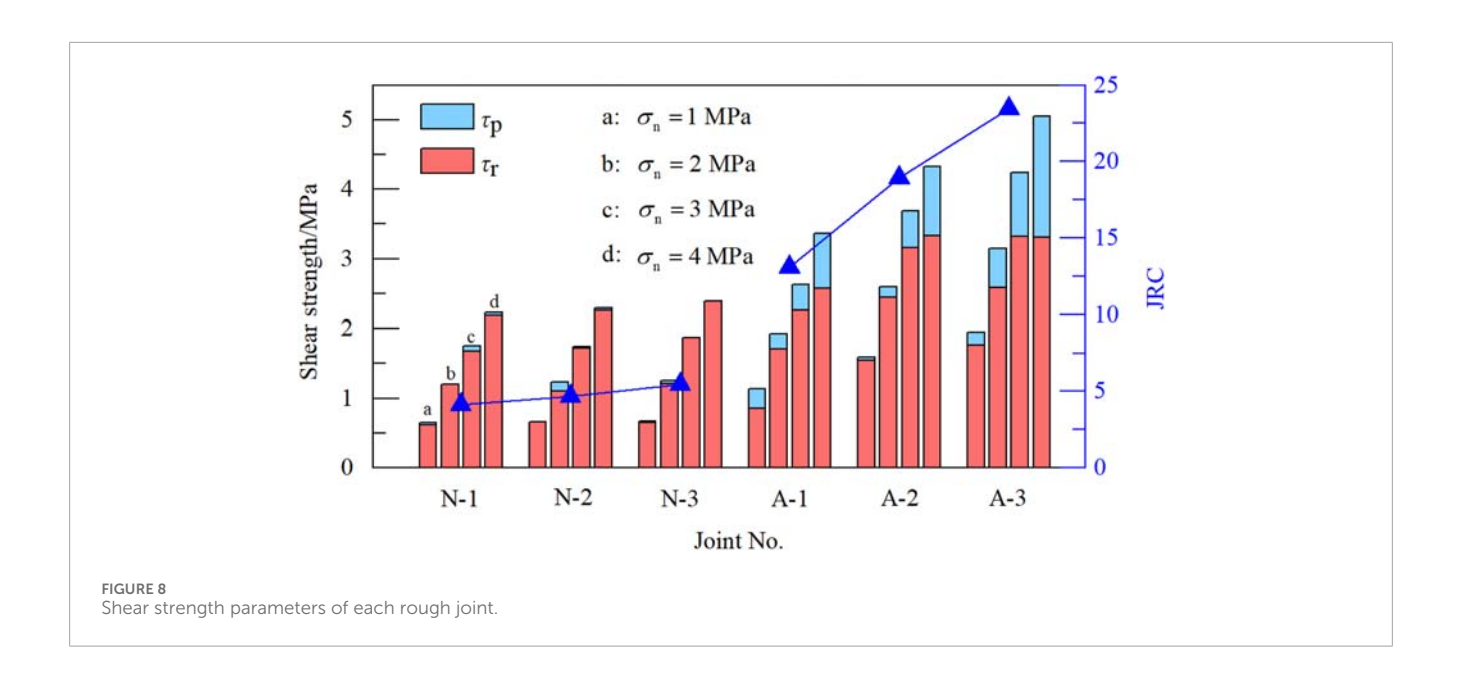
Note: Shear strength reduction= $(\tau_{\text{p-measured}} - \tau_{\text{r-measured}})/\tau_{\text{p-measured}} \times 100\%$.

portion of each tension joint were extracted. DEMs representing the morphology of natural sandstone tension joints N-1, N-2, and N-3 were constructed in Figure 4b. To ensure consistency with the artificial fractal joints, the DEMs were re-sampled with an interval of $\Delta=0.78125$ mm, resulting in uniformly distributed points (129 points per side) on the *XOZ* plane. Specimens containing natural sandstone tension joints N-1, N-2, and N-3 were 3D printed and cast following the methodology in Section 2.1 and 2.2.

2.4 Joint roughness quantification

Barton introduced the Joint Roughness Coefficient (JRC) to characterize rock joint roughness, proposing the empirical peak shear strength criterion of rough joints as Equation 1:

$$\tau_{\rm p} = \sigma_{\rm n} \tan \left(\rm JRC \, lg \, \frac{\rm JCS}{\sigma_{\rm n}} + \varphi_{\rm b} \right)$$
 (1)





where, $\tau_{\rm p}$ (MPa) is the peak shear strength; $\sigma_{\rm n}$ (MPa) is the normal stress; JCS (MPa) is the joint wall compressive strength, $\varphi_{\rm b}$ (°) is the basic friction angle of the material.

Adopted as the standard roughness parameter by ISRM (1978), JRC serves as the primary reference in rock joint shear studies (Singh and Basu, 2016; Singh and Basu, 2017; Liu et al., 2019; Zheng et al., 2020). Alternatively, Tse and Cruden (1979) quantified 2D roughness along the shear direction using the root mean square Z_2 (Equation 2), and constructed a fitting equation for calculating JRC^{2D} (Equation 3).

$$Z_{2} = \sqrt{\frac{1}{m-1} \sum_{i=1}^{m-1} \left(\frac{h_{i+1} - h_{i}}{\Delta}\right)^{2}}$$
 (2)

$$JRC^{2D} = 32.2 + 32.47 \lg Z_2 \tag{3}$$

where, h_i is the height at the *i*th point on the joint profile, m is the number of measuring points along the shear direction, and Δ is the sampling interval along shear direction. Figure 5 illustrates

these parameters under the specified shear direction (positive z-axis orientation).

Consequently, the three-dimensional joint roughness coefficient JRC^{3D} can be quantified as Equation 4:

$$JRC^{3D} = \frac{1}{m} \sum_{i=1}^{m} JRC_{i}^{2D}$$
 (4)

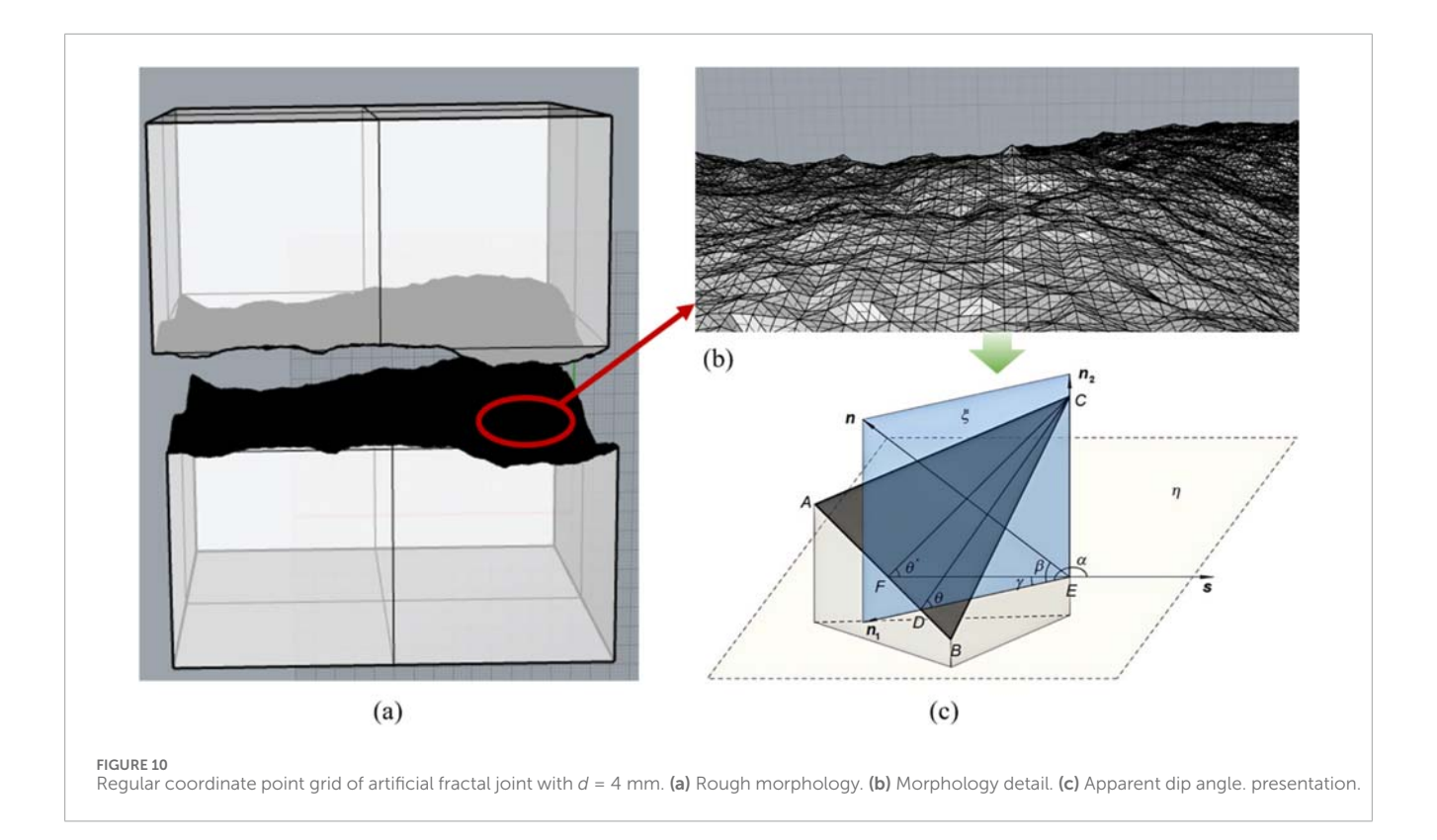
where, m is the number of 2D profiles sampled across the joint surface parallel to the shear direction (m = 129 in this study); JRC_i^{2D} is the ith JRC^{2D} regressed by Z₂. The shear-direction-dependent JRC^{3D} quantified by Z₂ is presented in Table 1.

3 Conduction of direct shear tests

3.1 Direct shear test performance

Direct shear tests were performed on well-matched joint specimens comprising: (a) natural tension joints (N-1, N-2, N-3) and (b) artificial fractal joints (A-1, A-2, A-3) in accordance with the revised ISRM Suggested Method (Muralha et al., 2014). Constant normal load (CNL) conditions were applied perpendicular to the rock joints, simulating near-surface rock mass boundary conditions where joint-parallel shear displacement and normal-direction dilatancy remain unconstrained (Lam and Johnston, 1989).

Tests were performed using the gear-driven direct shearing apparatus as shown in Figure 6a. The load and displacement condition on the rough joints are shown in Figures 6b,c. A constant horizontal displacement rate (0.02 mm/s) was imposed on the upper specimen half through a roller boundary connected to the vertical load cell, while the lower half remained fixed. Constant vertical stress was maintained throughout shearing. The shear direction aligned with the *z*-axis positive direction, i.e., the shear vector s=(0, 0, 1). Four normal stress levels at σ _n = 1 MPa, 2 MPa, 3 MPa and 4 MPa were selected based on typical stress ranges in excavation practice (Barton and Shen, 2017).



The shear load (T) and normal load (N) were continuously recorded by the load cells with a maximum load range of 500 kN. Shear displacement (u), which is parallel to the shear direction) was continuously measured using linear variable differential transformers (LVDTs) with a maximum range of 10 mm. Data acquisition employed a JM3183 multifunctional static strain testing system with Yangzhou Jingming software (Ver. 8.8) at 1 Hz sampling frequency. To quantify roughness-driven stress concentration, red marker was applied to the upper half joint surface for deformation pattern monitoring (Figure 6d). Testing terminated at u=6 mm displacement, corresponding to the residual shear stage onset.

3.2 Direct shear test results

Figure 7 illustrates shear stress (τ) versus shear displacement(u) relationships for joints with varying morphologies under CNL conditions. Shear parameters of joint specimens under various normal stresses are presented in Table 2 and Figure 8. Consistent with visual observations of artificial fractal surfaces and natural sandstone tension joints in Section 2, it could be roughly recognized that:

- 1. Natural sandstone tension joints exhibit comparable peak shear strength (τ_p) under identical CNL condition, which is coincide with their similar roughness. Besides, shear stresses keep constant to residual stages as $\tau_r = \tau_p$ (τ_r is the residual shear strength) when u approaches 6 mm.
- 2. Artificial fractal joints with higher d values, demonstrate significantly greater $\tau_{\rm p}$ under equivalent CNL conditions. At $\sigma_{\rm n}$

= 3 MPa and 4 MPa, rougher artificial joints exhibit post-peak strength reduction before reaching residual states.

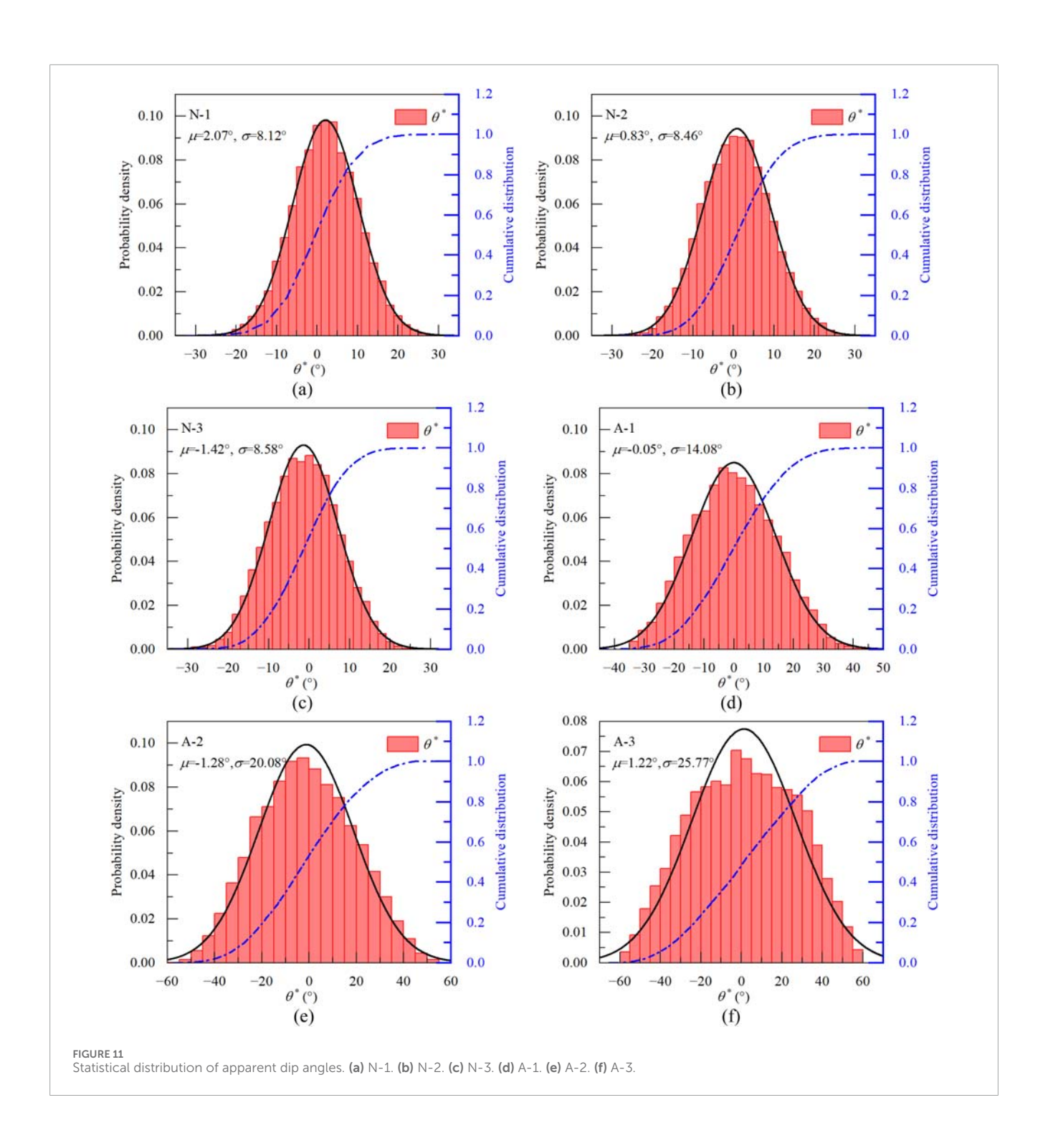
It is obtained that the damage sensitivity correlates with joint roughness and normal stress magnitude (Jiang et al., 2020). Consequently, rougher joints under higher $\sigma_{\rm n}$ exhibit more pronounced post-peak strength reduction. Asperity damage degrades original morphology, diminishing roughness contributions to residual strength. For developing a new $\tau_{\rm p}$ criterion based on morphological parameters, this study neglects post-peak behavior to simplify analysis. The derivation consequently focuses on correlating directional morphological characteristics with $\tau_{\rm p}$.

The influence of θ^* spatial distribution on joint roughness during shearing was analyzed through interfacial interactions under normal and shear loads. Contact areas, traced by red mark, was systematically recorded via photography at peak shear strength displacement (Figure 9). Quantitative analysis reveals that: (1) significant interfacial traces occur exclusively on asperities facing the shear direction, and (2) primary shear failure initiates at high positive- θ^* asperities, independent of elevation.

4 Shear criterion revised by 3D joint morphological features

4.1 Statistical parameters of apparent dip angle

While JRC-based indices exhibit limitations in characterizing joint morphological details under shear, alternative joint



roughness parameters have been proposed. Grasselli and Egger (2003) introduced statistical distribution parameters of apparent dip angle (θ^*) to quantify anisotropic 3D joint morphology. This framework establishes that τ_p coincides with crushing of asperities possessing critical θ^* . Subsequent to τ_p , progressive degradation of joint morphology reduces shear strength with increasing u. Notably, tests under higher normal stresses and greater initial roughness exhibited more pronounced roughness reduction.

Section 2 details the reconstruction of rough joint surfaces presented by regular triangular elements (Figure 10a). For each asperity, θ^* is defined as the angle between the shear-direction vector and the asperity facet (Figures 10b,c), where η is the shear plane; ξ is the plane perpendicular to the triangle element; n is the outward normal vector of the triangle element; n is the shear vector; n is the component of n that parallel to the shear plane; n is the component of n that perpendicular to the shear plane; n is the dip angle (°); n is the azimuth angle measured clockwise from n to n to n (°).

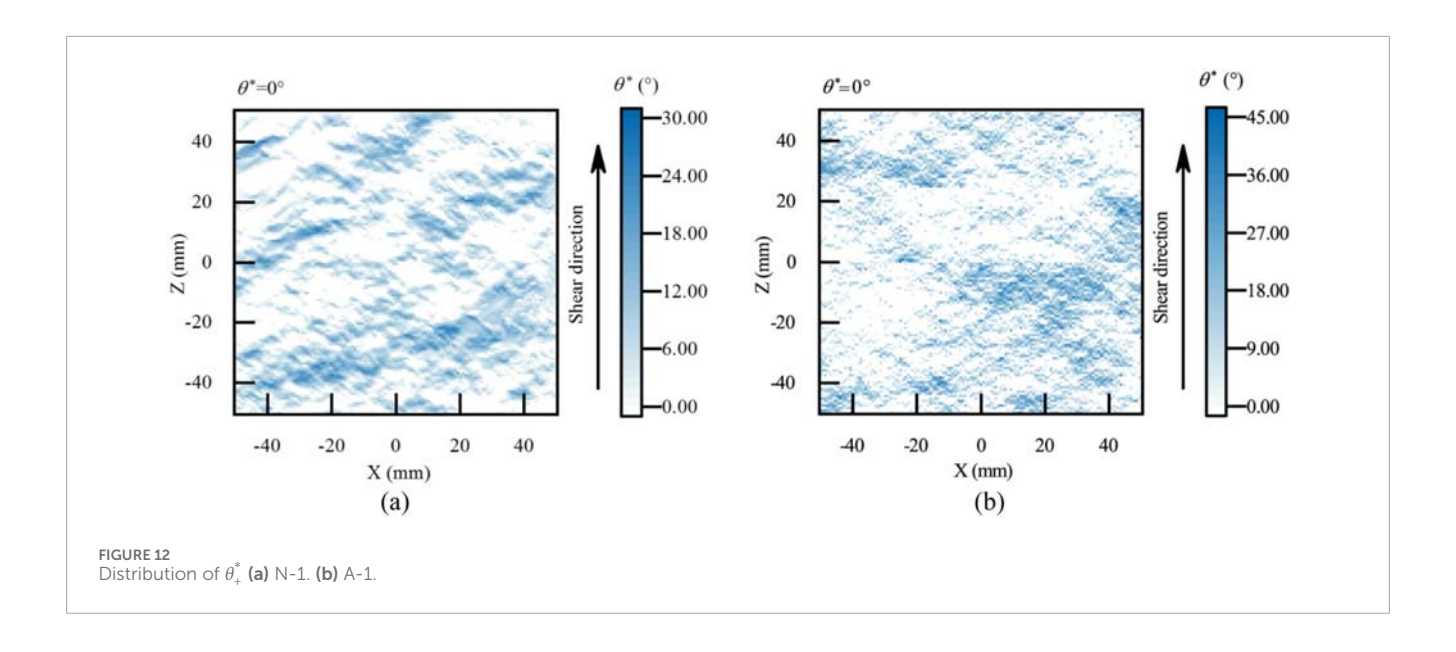


TABLE 3 θ^* -related roughness parameter obtained from joint morphologies.

Joint no.	A ₀ /%	θ _{max} */(°)	С	R ²	$\frac{\theta_{max}^*}{C}/()$	$\frac{\theta_{max}^*}{C+1}/(\mathring{})$
N-1	58.64	27.71	2.99	0.9988	9.28	6.95
N-2	50.59	30.72	3.77	0.9987	8.15	6.44
N-3	43.21	28.07	3.58	0.9987	7.84	6.13
A-1	49.23	43.72	2.87	0.9982	15.26	11.31
A-2	46.79	56.36	2.54	0.9986	22.17	15.91
A-3	51.75	64.65	2.02	0.9960	31.97	21.39

The geometric determination of θ^* is shown as Equation 5:

$$\tan \theta^* = -\tan \theta \cos \alpha \tag{5}$$

When the shear vector \mathbf{s} is anti-parallel to \mathbf{n}_1 , which means that $\alpha = \pi$, θ^* reduces to the two-dimensional dip angle θ . It is proposed that in the process of joint shearing, surfaces that are squeezed together exhibit $\theta^* > 0^\circ$ (i.e., θ_+^*), while surfaces separated from each other exhibit $\theta^* < 0^\circ$. Figure 11 presents the statistical distribution of θ^* under $\mathbf{s} = (0, 0, 1)$. The distribution of parameter θ^* can be approximated by a Gaussian distribution with an average value μ and a standard deviation σ . Figure 12 illustrates the spatial distribution of θ_+^* on joint surfaces under identical shear conditions.

4.2 Verification of the proposed peak shear strength criteria

Two parameters (a) maximum apparent dip angle θ^*_{\max} and (b) roughness parameter C (where C > 1) (Chen et al., 2021a) quantifying θ^* distribution, were introduced to refine Grasselli's

peak shear strength criterion (Grasselli and Egger, 2003; Grasselli, 2006). The expression of the peak shear strength of rough joints is shown as Equation 6:

$$\tau_{\rm p} = \left[1 + \exp\left(-\frac{1}{9A_0} \frac{\theta_{\rm max}^*}{C} \frac{\sigma_{\rm n}}{\sigma_{\rm t}}\right)\right] \sigma_{\rm n} \tan\left[\varphi_{\rm b} + \left(\frac{\theta_{\rm max}^*}{C}\right)^{1.18\cos(\beta)}\right] \tag{6}$$

where, $A_0 = A_{\rm shear}/A$ represents the maximum normalized contact area calculated for a threshold apparent dip angle of 0°, the value of which is typically very close to 50%. $A_{\rm shear}$ (mm²) is the total area that facing the shear direction, i.e., the total area of asperities with positive apparent dip angles θ_+^* . A (mm²) is the total area of the rough joint surface; $\sigma_{\rm t}$ (MPa) is the tensile strength of the intact rock; β (°) is the angle between the normal direction of the joint and the schistosity plane ($\beta = 0^\circ$ for non-schistose specimens). C is a roughness parameter derived from Equation 7:

$$A_{\theta^*} = A_0 \left(\frac{\theta_{\text{max}}^* - \theta^*}{\theta_{\text{max}}^*} \right)^C \tag{7}$$

where, A_{θ^*} is the normalized area with apparent dip angles exceed θ^* . θ^*_{max} (°) is the maximum apparent dip angle along the shear direction. Higher C values indicate reduced potential contact area during shearing, diminishing shear resistance. θ^*_{max}/C shows positive correlation with 3D roughness of joints, thus serves as Grasselli and Egger (2003), Grasselli (2006) joint roughness metric

Tatone and Grasselli (2009), Tatone and Grasselli (2014) derived the definite integral of Equation 7 as Equation 8:

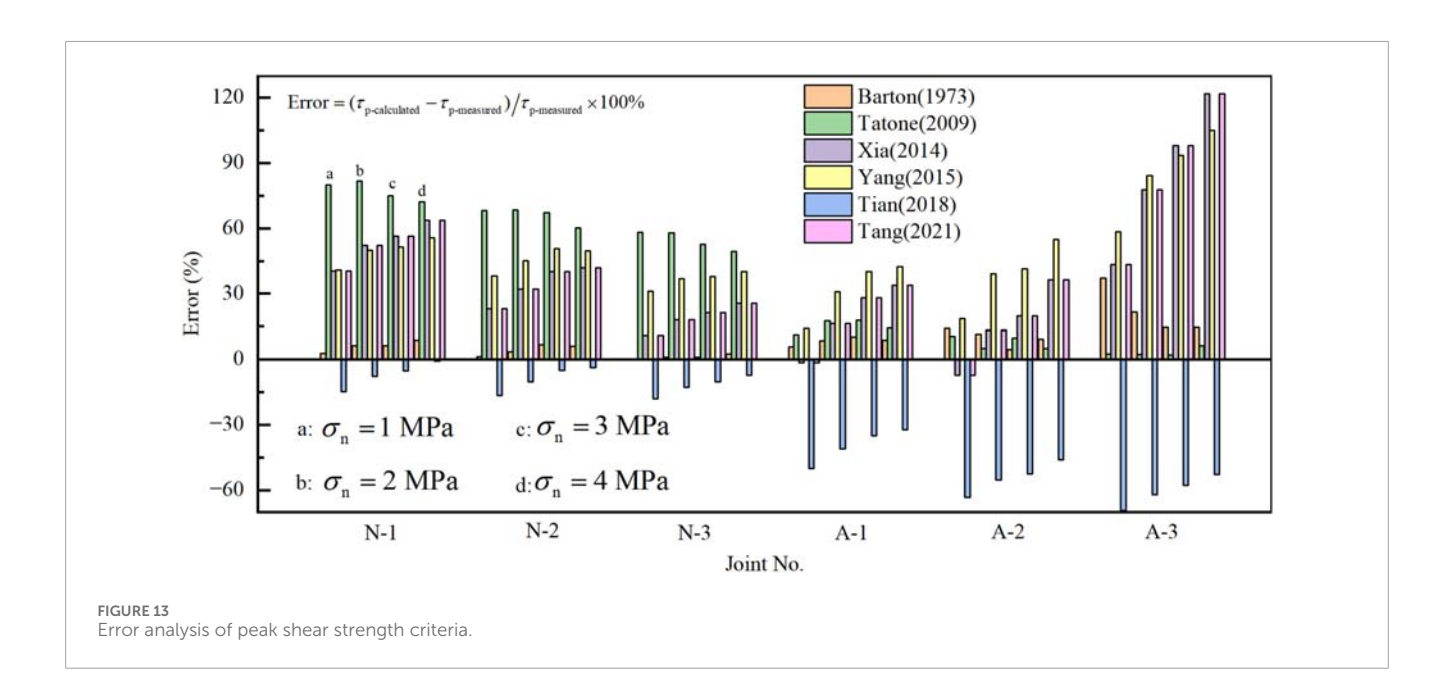
$$\int_{0}^{\theta_{\text{max}}^*} \left(\frac{\theta_{\text{max}}^* - \theta^*}{\theta_{\text{max}}^*}\right)^{C} d\theta^* = -\left(\frac{\theta_{\text{max}}^*}{C+1}\right) \cdot \left(\frac{\theta_{\text{max}}^* - \theta^*}{\theta_{\text{max}}^*}\right)^{C+1} \Big|_{0}^{\theta_{\text{max}}^*} = \frac{\theta_{\text{max}}^*}{C+1}$$
(8)

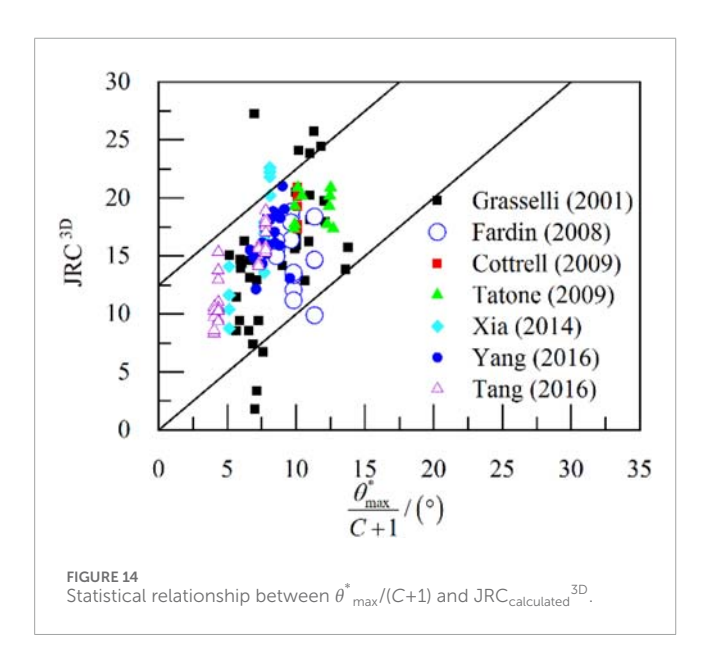
 $\theta^*_{\rm max}/(C+1)$ is reformulated to better characterize joint morphology. It was suggested that a larger value of $\theta^*_{\rm max}/(C+1)$ is representative of a greater proportion of steeply dipping triangles and hence a rougher joint surface morphology under

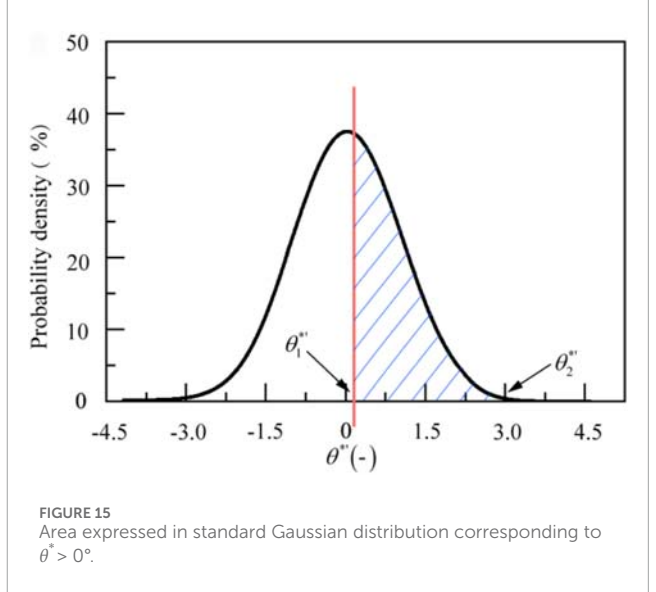
TABLE 4 Peak shear strength criteria proposed on the basis of parameter C.

References	Peak shear strength criterion
Tatone and Grasselli (2009)	$\tau_{\rm p} = \left[1 + \exp\left(-\frac{1}{9A_0} \cdot \frac{\theta_{\rm max}^*}{C+1} \cdot \frac{\sigma_{\rm n}}{\sigma_{\rm t}}\right)\right] \cdot \sigma_{\rm n} \cdot \tan\left(\varphi_{\rm b} + \left(\frac{\theta_{\rm max}^*}{C+1}\right)^{1.34f^{0.058}}\right)$
Xia et al. (2014)	$\tau_{\mathrm{p}} = \sigma_{\mathrm{n}} \cdot \tan \left\{ \varphi_{\mathrm{b}} + \frac{4A_{\mathrm{0}}\theta_{\mathrm{max}}^{3}}{C+1} \left[1 + \exp \left(-\frac{1}{9A_{\mathrm{o}}} \cdot \frac{\theta_{\mathrm{max}}^{2}}{C+1} \cdot \frac{\sigma_{\mathrm{n}}}{\sigma_{\mathrm{t}}} \right) \right] \right\}$
Yang et al. (2015)	$ au_{ m p} = \sigma_{ m n} \cdot an \left[arphi_{ m b} + rac{ heta_{ m max}^*}{C^{0.45}} \cdot \exp \left(-rac{\sigma_{ m a}}{ m JCS} { m C}^{0.75} ight) ight]$
Tian et al. (2018)	$ au_{ m p} = \sigma_{ m n} \cdot an \Big(arphi_{ m b} + rac{160 \cdot C^{\prime - 0.44}}{\sigma_{ m n}/\sigma_{ m r} + 2} \Big)$
Tang et al. (2021)	$\tau_{\mathrm{p}} = \left[1 + \left(0.13 - 0.012 \frac{A_0 \theta_{\mathrm{max}}^*}{C+1}\right) \ln\left(\mathrm{JSC}\right)\right] \sigma_{\mathrm{n}} \cdot \tan\left[\varphi_{\mathrm{b}} + \frac{4A_0 \theta_{\mathrm{max}}^*}{C+1}\left[1 + \exp\left(-\frac{1}{9A_0} \cdot \frac{\theta_{\mathrm{max}}^*}{C+1} \cdot \frac{\sigma_{\mathrm{n}}}{\sigma_{\mathrm{t}}}\right)\right]\right]$

Note: l is the sampling interval; C' is the updated distribution parameter calculated by equation $\theta^*_{\max}/(C+1) = 90^\circ/(C'+1)$; JSC, is the joint wall strength difference coefficient; JSC, 1 for homogeneous joint walls.







Joint no.	μ/(°)	σ/(°)	$\theta_1^{*!}$	$\theta_2^{*!}$	ϕ (θ_1^* ')	$\Phi(\theta_1^*)$	E (θ*')	<i>E</i> (θ* θ*> 0°)/(°)	E (θ* θ*> 0°)-μ/(°)
N-1	2.07	8.12	-0.25	3.00	0.3867	0.4013	0.65	7.31	5.24
N-2	0.83	8.46	-0.10	3.00	0.3970	0.4602	0.74	7.05	6.22
N-3	-1.42	8.58	0.17	3.00	0.3932	0.5675	0.91	6.38	7.80
A-1	-0.05	14.08	0.00	3.00	0.3989	0.5000	0.80	11.18	11.23
A-2	-1.28	20.08	0.06	3.00	0.3983	0.5239	0.84	15.52	16.80
A-3	1.22	25.77	-0.05	3.00	0.3986	0.4801	0.77	20.98	19.76

TABLE 5 Probability distribution parameters of θ^* .

a certificate shear direction. Table 3 presents the θ^* -related roughness parameter obtained from joint morphologies, and Table 4 summarizes additional peak shear strength criteria incorporating parameter C.

As shown in Figure 13, the prediction accuracy of different criteria for the peak shear strength of joints with varying roughness differs significantly (prediction effectiveness is evaluated within $\pm 30\%$ error): Barton criterion exhibits the closest agreement with experimental results; Tatone criterion performs well for high-roughness joints but poorly for low-roughness cases; Tian criterion shows good fitting for low-roughness joints but fails under high-roughness conditions; Xia criterion and Tang criterion (equivalent to Xia criterion when JSC = 1) are applicable to moderately rough joints; while Yang criterion yields low prediction accuracy across all roughness levels.

The significant errors observed in these criteria primarily stem from three sources:

- 1. Parameter sensitivity. It is important to note that unavoidable errors exist in peak shear strength criteria when considering θ^*_{\max} and C. θ^*_{\max} exhibits significant sensitivity to modeling interval and 3D printing accuracy, with values potentially approaching 90° under high-resolution conditions. In contrast, C demonstrates greater consistency (Magsipoc et al., 2019).
- 2. Limited applicability of the criterion's physical meaning. For instance, when applying Grasselli and Tatone's equations to joints with smooth morphologies (i.e., $\theta^*_{\rm max}\!\!\to\!\!0$), it is obtained that $\tau_p\!\!\to\!\!2\sigma_n tan$ $(\phi_b).$ This result contradicts the Mohr-Coulomb criterion, which explains the anomalously high errors observed in natural sandstone tension joints exhibiting low roughness.
- 3. Narrow roughness range in calibration process. Figure 14 summarizes the statistics the statistics of $\theta^*_{\rm max}/(C+1)$ and the JRC^{3D} in scholars' papers. To mitigate sampling-interval-induced variations in $\theta^*_{\rm max}$ and C, datasets with sampling interval $l=0.25-0.5\,{\rm mm}$ were selected. The JRC^{3D} values predominantly fall within 8–20. Different criteria are applicable to distinct ranges of joint roughness.

4.3 Modification of peak shear strength criterion of rough joints

4.3.1 Substitution of θ^*_{max} and $\theta^*_{\text{max}}/(C+1)$

The subjective factors involved in determining θ^*_{\max} may introduce additional errors. The apparent dip angles θ^* are assumed to follow a Gaussian distribution characterized by mean value μ and standard deviation σ , i.e., $\theta^* \sim N$ (μ , σ^2). According to the Pauta criterion (3σ principle), 99.74% of data fall within (μ – 3σ , μ + 3σ) is 0.9974. Data beyond this range (<0.26% probability) are considered outliers and should be excluded. Consequently, an equivalent maximum dip angle is defined as $\theta^*_{\max-eq} = \mu + 3\sigma$.

Based on the power relationship between θ^* and A_{θ^*} mentioned by Grasselli, only shear-facing apparent dip angles θ^*_+ ($\theta^* > 0^\circ$) are considered in the τ_p calculation. Assume θ^*_+ is an independent variable, Equation 7 can be further modified as Equation 9:

$$F(\theta_{+}^{*}) = \frac{A_{\theta_{+}^{*}}}{A_{0}} = \left(\frac{\theta_{\text{max-eq}}^{*} - \theta_{+}^{*}}{\theta_{\text{max-eq}}^{*}}\right)^{C}$$
(9)

Where, $F(\theta_+^*)$ is the complementary cumulative distribution function of θ_-^* .

A probability density function $g(\theta_+^*)$ was developed to characterize the distribution of $g(\theta_+^*)$. It can be expressed as Equation 10:

$$g(\theta_{+}^{*}) = -F'(\theta_{+}^{*}) = -\frac{\mathrm{d}A_{\theta_{+}^{*}}}{A_{0}\mathrm{d}\theta_{+}^{*}} = \frac{C}{\theta_{\mathrm{max-eq}}^{*}} \left(\frac{\theta_{\mathrm{max-eq}}^{*} - \theta_{+}^{*}}{\theta_{\mathrm{max-eq}}^{*}}\right)^{C-1} \tag{10}$$

The expectation of θ_+^* is expressed as Equation 11:

$$E(\theta_{+}^{*}) = \int_{0}^{\theta_{\text{max}-eq}^{*}} \theta_{+}^{*} g(\theta_{+}^{*}) d\theta_{+}^{*} = \frac{\theta_{\text{max}-eq}^{*}}{C+1}$$
 (11)

Therefore, $\theta^*_{max}/(C+1)$ is proved to be equivalent to the expectation of θ^*_+ (Chen et al., 2021b). This probabilistic framework provides a more efficient method for deriving the representative joint surface parameter $\theta^*_{max}/(C+1)$.

 $E(\theta_+^*)$ could be calculated based on the distribution of variable θ^* as the conditional expectation of $\theta^* > 0^\circ$ ($E(\theta^* | \theta^* > 0^\circ)$). The Gaussian distribution $\theta^* \sim N$ (μ , σ^2) could be converted to standard Gaussian distribution as $\theta^{*'} \sim N$ (0, 1), where $\theta^{*'} = (\theta^{*'} - \mu)/\sigma$. Consequently, the interval $0^\circ < \theta^* < \mu + 3\sigma$ could be expressed as $-\mu/\sigma < \theta^{*'} < 3$. The corresponding range is represented as the shadow area in Figure 15.

TABLE 6 $\tau_{\rm p}$ calculated by the modified peak shear strength criterion.

Joint. No	$\sigma_{\sf n}/{\sf MPa}$	$ au_{ extsf{p-measured}}/ extsf{MPa}$	$E(\theta^* \theta^*>0^\circ)-\mu/(\circ)$	$ au_{ extsf{p-calculated}}/ extsf{MPa}$	Error/%
	1	0.65		0.59	-9.43
X 1	2	1.20	5.24	1.14	-4.67
N-1	N-1 3 1.75	5.24	1.69	-3.60	
	4	2.23		2.22	-0.36
	1	0.66		0.64	-2.40
N 2	2	1.23	622	1.24	0.41
N-2	3 1.74	6.22	1.81	3.83	
	4	2.29		2.37	3.32
	1	0.67		0.74	10.46
N-3	2 1.26	7.80	1.39	10.35	
IN-3	3	1.84	7.80	2.01	9.21
	4	2.37		2.61	10.07
	1	1.14		0.99	-13.54
A-1	2	1.93	11.23	1.77	-8.08
A-1	3	2.63	11,23	2.50	-4.92
	4	3.36		3.19	-5.09
	1	1.59	16.80	1.58	-0.56
A-2	2	2.60		2.61	0.42
A-Z	3	3.69	10.00	3.52	-4.68
	4	4.32		4.35	0.71
	1	1.95		2.11	8.26
A-3	2	3.15	19.76	3.25	3.12
11-3	3	4.24	12.70	4.24	-0.04
	4	5.05		5.14	1.76

Note: Error = $[(\tau_{p\text{-calculated}} - \tau_{p\text{-measured}})/\tau_{p\text{-measured}}] \times 100\%$.

The conditional expectation of $\theta^{*'}$ $(-\mu/\sigma < \theta^{*'} < 3)$ could be calculated as Equation 12:

$$E(\theta^{*'}|\theta_{1}^{*'} < \theta^{*'} < \theta_{2}^{*'}) = \int_{-\infty}^{+\infty} \theta^{*'} \phi_{\theta^{*'}|\theta_{1}^{*'} < \theta^{*'} < \theta_{2}^{*'}} (\theta^{*'}) d\theta^{*'}$$

$$= \int_{\theta_{1}^{*'}}^{\theta_{2}^{*'}} \frac{\theta^{*'} \phi(\theta^{*'})}{P(\theta_{1}^{*'} < \theta^{*'} < \theta_{2}^{*'})} d\theta^{*'}$$

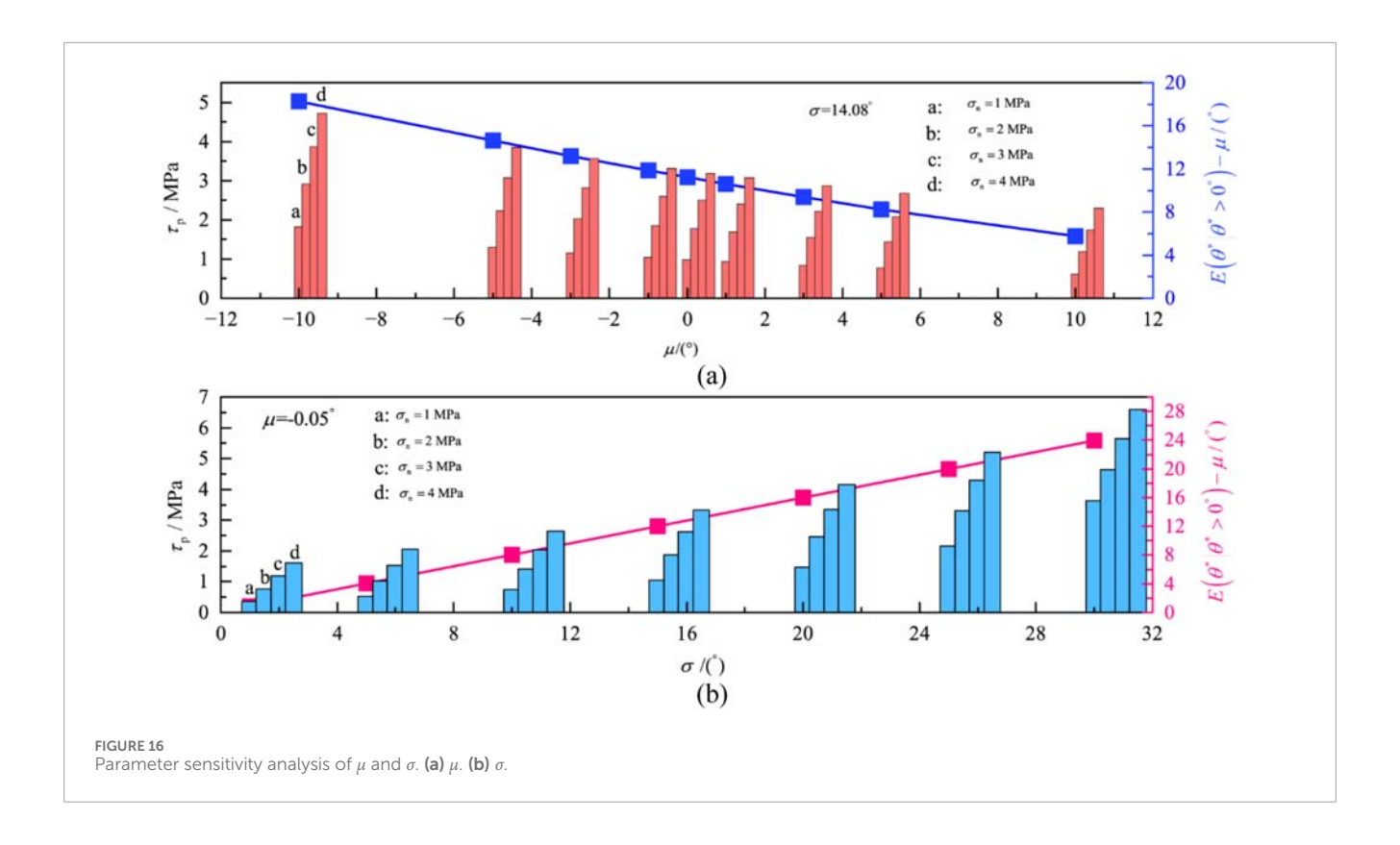
$$= \frac{\phi(\theta_{1}^{*'}) - \phi(\theta_{2}^{*'})}{\Phi(\theta_{2}^{*'}) - \Phi(\theta_{1}^{*'})}$$
(12)

Where, $g(\theta^{*'})$ is the probability density function of standard Gaussian distribution, $\theta_1^{*'} = -\mu/\sigma$, $\theta_2^{*'} = 3$, $\phi()$ and $\Phi()$ are

the probability density function and the cumulative distribution function of Gaussian distribution, respectively $(\phi(3) = 0, \Phi(3) = 1)$; $P(\theta_1^{*'} < \theta^{*'} < \theta_2^{*'})$ is the probability of $\theta_1^{*'} < \theta^{*'} < \theta_2^{*'}$ ($P(\theta_1^{*'} < \theta^{*'} < \theta_2^{*'})$). Table 5 presents the probability distribution parameter values in the calculation of $E(\theta^* | \theta^* > 0^\circ)$.

4.3.2 Modification of peak shear strength criterion

The Mohr-Coulomb strength criterion provides the basis for modeling the shear properties of rough joints. For non-consecutive rough joints where cohesion c is negligible, the friction angle is



governed by joint roughness. Consequently, a peak shear strength criterion derived from this framework must be modified to account for complex joint morphological characteristics. A significant limitation is revealed: low-roughness joints (N-1, N-2, N-3) exhibit opposite trends of variation in $E(\theta^*|\theta^*>0^\circ)$ -JRC^{3D}. To preserve the physical significance of peak shear strength criterion at low-roughness joints, parameter $E(\theta^*|\theta^*>0^\circ)$ - μ is introduced as a shear-direction-dependent joint roughness metric. Fitting results demonstrate a strong linear relationship between $E(\theta^*|\theta^*>0^\circ)$ - μ and JRC^{3D} ($R^2=0.9819$). Thus, the peak shear strength criterion is modified as:

$$\tau_{\text{p-calculated}} = \sigma_{\text{n}} \tan \left\{ \left[1.27 \left(E(\theta^* | \theta^* > 0^{\circ}) - \mu \right) - 4.29 \right] \cdot \lg \frac{\text{JCS}}{\sigma_{\text{n}}} + \varphi_{\text{b}} \right\}$$
(13)

Where $\tau_{\text{p-calculated}}$ is the peak shear strength predicted by the modified criterion. The results are shown in Table 6. It should be noticed that this criterion is regressed based on the statistical morphological parameters specific to the rough joints studied in this paper. Applying this criterion to joints with different sampling resolution may alter the coefficient values in Equation 13. Further studies is required to develop a generalized $E\left(\theta^* \middle| \theta^* > 0^\circ\right)$ - μ -related peak shear strength criterion.

Parameters μ and σ serves as key indicators reflecting the shear-direction-dependent joint roughness. Parameter sensitivity analysis is performed to analyze the influence of μ and σ on the joint roughness character E ($\theta^* | \theta^* > 0^\circ$)- μ and the peak shear strength τ_p . Figure 16 illustrates the correlation trends between E ($\theta^* | \theta^* > 0^\circ$)- μ and τ_p under varying parameters μ and σ , respectively. It can be observed that: (1) With σ held constant, an increase in μ leads to a decrease in E ($\theta^* | \theta^* > 0^\circ$)- μ , resulting in reduced τ_p under identical

normal stress conditions. This aligns with the pattern shown in N-1, N-2, N-3. (2) With μ held constant, an increase in σ elevates the value of $E(\theta^*|\theta^*>0^\circ)$ - μ , corresponding to enhanced τ_p . This aligns with the pattern shown in N-1, A-1, A-2, A-3.

4.3.3 Validation of the modified model

To validate the accuracy and applicability of the joint shear strength criterion, direct shear test results for concrete specimens with rough joints from publications by Xia (Xia et al., 2014) and Tang (Tang et al., 2016) were selected. The corresponding joint morphological parameters, fundamental physical-mechanical properties of materials, and stress states were substituted into Equation 13, and the comparison between the calculated results and the experimental data are presented in Table 7. The selected test data satisfy the following conditions:

- 1. The statistical mean of apparent dip angles μ is near 0°;
- 2. Normal stress levels σ_n range from 1 to 4 MPa;
- 3. Specimen dimensions are comparable to those used in this study, minimizing size effects;
- Sampling intervals for joint morphology characterization are within the same order of magnitude as those adopted in this paper.

Due to insufficient reporting of statistical parameters μ and σ for apparent dip angles in the cited publications, these critical values were derived from available datasets based on Equations 14, 15:

$$\frac{0-\mu}{\sigma} = 1 - A_0 \tag{14}$$

$$\theta_{\text{max}}^* = \mu + 3\sigma \tag{15}$$

TABLE 7 Verification of the modified peak shear strength criterion.

References Joint No. $\sigma_{\rm c} = \varphi_{\rm b}/({}^{\circ})$	Joint No.	$\sigma_{\rm c}$	φ _b /()		Statist	Statistical parameters of $ heta^*$	meters	of $ heta^*$	σ_{n}	$ au_{ extsf{p-measured}}$	Tp-calculated	Error/%
		/MPa		A ₀ (-)	θ max /()	z°,	σ /(°)	$E(\theta^{\dagger} \theta^{>}0)^{-}\mu/(0)$	/MPa	/MPa	/MPa	
									1.00	1.19	1.57	32.09
	+	1	Ĺ	000	Ç	S	1		1.50	1.77	2.12	20.03
	<u></u>	27.50	ક	0.499	99.00	0.00	19.6/	15.69	2.00	2.24	2.64	17.71
(100)									3.00	2.84	3.58	26.16
Ala et al. (2014)									1.00	1.75	1.89	8.24
		i i	L C	i c			6		1.50	2.20	2.48	12.77
	11-(05.72	çç	0.504	69.30	0.23	72.07	18.22	2.00	2.78	3.02	8.62
									3.00	3.34	4.00	19.88
									1.20	1.11	1.10	-0.49
	J -IV $^+$	16.10	31	0.513	44.70	0.44	14.75	11.49	1.60	1.44	1.41	-2.25
									2.00	1.71	1.70	-0.68
									1.20	1.12	1.11	-0.48
	J-IV	16.10	31	0.501	43.90	0.00	14.63	11.67	1.60	1.41	1.42	0.64
()100) [1-1-1-E									2.00	1.67	1.71	2.45
tang et al. (2016)									1.20	1.48	1.66	12.03
	J-V ⁺	16.10	31	0.534	78.40	1.29	25.45	19.49	1.60	1.86	2.01	8.31
									2.00	2.23	2.35	5.22
									1.20	1.37	1.69	23.55
	J-V-	16.10	31	0.506	75.60	0.25	25.12	19.88	1.60	1.71	2.05	19.94
									2.00	2.01	2.38	18.61
Note: Frror = [(r	x-:	.1~100%										

Note: Error = [($\tau_{\text{p-calculated}} - \tau_{\text{p-measured}}$)/ $\tau_{\text{p-measured}}$]×100%.

Table 7 indicates minimal discrepancies between predicted and measured $\tau_{\rm p}$ values. This demonstrates the feasibility of establishing joint shear strength criteria using shear direction-dependent roughness parameters to predict peak shear strength.

5 Conclusion

The three-dimensional morphological characteristics of joint surfaces significantly influence the shear strength behavior of rock joints. This paper investigated the relationship between the shear strength of joints, joint roughness, and normal stress levels through direct shear tests on joint specimens with varying 3D roughness. A new parameter was proposed to describe shear-direction-dependent joint roughness, and a modified criterion for calculating the peak shear strength of joints was established. The main conclusions are as follows:

- Digital elevation models of fractal joints and natural sandstone tension joints were solidified into physical joint models with distinct morphological features using 3D printing technology. Well-matched joint specimens replicating sandstone, containing varied 3D morphological characteristics, were successfully cast using cement-based rock-like materials. The results demonstrate that this process produces homogeneous joint specimens with well-defined morphological features.
- 2. Direct shear tests under constant normal load (CNL) conditions were conducted on the well-matched joint specimens. The differences in peak shear strength and shear stress-displacement curves for joints of varying roughness were analyzed. Key observations prove that: a) under identical normal stress, peak shear strength increases significantly with higher joint roughness; b) higher normal stress levels lead to more pronounced shearing-off of local asperities and more distinct post-peak shear stress reduction behavior.
- 3. Conventional joint roughness parameters were calculated, and existing shear strength criteria proposed by scholars were evaluated for prediction errors. This underscores the critical importance of selecting appropriate parameters for characterizing joint surface morphology in shear strength analysis.
- 4. A shear-direction-dependent joint roughness parameter was modified. A new parameter $E\left(\theta^{*}|\theta^{*}>0^{\circ}\right)-\mu$ was proposed to characterize joint roughness. By fitting the direct shear test results, a modified joint shear strength criterion conforming to the Mohr-Coulomb failure criterion was established. This new criterion provides accurate estimates of the peak shear strength for joints of varying roughness.

Data availability statement

The datasets used or analyzed during the current study are available from the corresponding author on reasonable request.

Author contributions

YS: Data curation, Formal Analysis, Project administration, Resources, Visualization, Writing – original draft, Writing – review and editing, Investigation, Supervision.

Funding

The author(s) declare that financial support was received for the research and/or publication of this article. This work was supported by the National Major Scientific Research Project: Deep Exploration in China (CN. Grant No. 2024ZD1004103).

Acknowledgments

The research was supported by School of Civil Engineering, Beijing Jiaotong University.

Conflict of interest

The author declares that the research was conducted in the absence of any commercial or financial relationships that could be construed as a potential conflict of interest.

Generative Al statement

The author(s) declare that no Generative AI was used in the creation of this manuscript.

Publisher's note

All claims expressed in this article are solely those of the authors and do not necessarily represent those of their affiliated organizations, or those of the publisher, the editors and the reviewers. Any product that may be evaluated in this article, or claim that may be made by its manufacturer, is not guaranteed or endorsed by the publisher.

References

- Alejano, L. R., Muralha, J., Ulusay, R., Li, C. C., Pérez-Rey, I., Karakul, H., et al. (2018). ISRM suggested method for determining the basic friction angle of planar rock surfaces by means of tilt tests. *Rock Mech. Rock Eng.* 51 (12), 3853–3859. doi:10.1007/s00603-018-1627-6
- Bai, B., Zhou, R., Yang, G., Zou, W., and Yuan, W. (2023). The constitutive behavior and dissociation effect of hydrate-bearing sediment within a granular thermodynamic framework. *Ocean. Eng.* 268 (8), 113408. doi:10.1016/j.oceaneng.2022.113408
- Bai, B., Zhang, B., Chen, H., and Chen, P. (2025). A novel thermodynamic constitutive model of coarse-grained soils considering the particle breakage. *Transp. Geotech.* 50, 101462. doi:10.1016/j.trgeo.2024.101462
- Ban, L., Zhu, C., Qi, C., and Tao, Z. (2019). New roughness parameters for 3D roughness of rock joints. *Bull. Eng. Geol. Environ.* 78 (6), 4505–4517. doi:10.1007/s10064-018-1394-3
- Ban, L., Du, W., Jin, T., Qi, C., and Li, X. (2021). A roughness parameter considering joint material properties and peak shear strength model for rock joints. *Int. J. Min. Sci. Technol.* 31 (3), 413–420. doi:10.1016/j.ijmst.2021.03.007
- Barton, N. (1973). Review of a new shear-strength criterion for rock joints. *Eng. Geol.* 7 (4), 287-332. doi:10.1016/0013-7952(73)90013-6
- Barton, N., and Shen, B. (2017). Risk of shear failure and extensional failure around over-stressed excavations in brittle rock. *J. Rock Mech. Geotechnical Eng.* 9 (2), 210–225. doi:10.1016/j.jrmge.2016.11.004
- Barton, N., Bandis, S., and Bakhtar, K. (1985). Strength, deformation and conductivity coupling of rock joints. *Int. J. Rock Mech. Min. Sci. and Geomechanics Abstr.* 22, 121–140. doi:10.1016/0148-9062(85)93227-9
- Brown, S. (1995). Simple mathematical model of a rough fracture. *J. Geophys. Res.* 100, 5941–5952. doi:10.1029/94jb03262
- Chang, C., Ju, Y., Xie, H., Zhou, Q., and Gao, F. (2017). Non-darcy interfacial dynamics of air-water two-phase flow in rough fractures under drainage conditions. *Sci. Rep.* 7, 4570. doi:10.1038/s41598-017-04819-x
- Chen, X., Zeng, Y., Ye, Y., Sun, H., Tang, Z., and Zhang, X. (2021a). The physical meaning of Grasselli's morphology parameters and its correlations with several other 2D fracture roughness parameters. *Int. J. Rock Mech. Min. Sci.* 145 (4), 104854. doi:10.1016/j.ijrmms.2021.104854
- Chen, X., Zeng, Y., Ye, Y., Sun, H., Tang, Z., and Zhang, X. (2021b). A simplified form of Grasselli's 3D roughness measure $\theta^* max/(C+1)$. Rock Mech. Rock Eng. 54 (8), 4329–4346. doi:10.1007/s00603-021-02512-0
- Ding, L., and Li, G. (2021). Research on peak shear strength criterion of rock joints based on the evolution of dilation angle. *Geotechnical Geol. Eng.* 39 (7), 4887–4900. doi:10.1007/s10706-021-01801-3
- Eberhardt, E. (2009). The complete ISRM suggested methods for rock characterization, testing and monitoring: 1974-2006. *Int. J. Rock Mech. Min. Sci.* 46 (8), 1396–1397. doi:10.1016/j.ijrmms.2009.06.002
- Fardin, N. (2008). Influence of structural non-stationarity of surface roughness on morphological characterization and mechanical deformation of rock joints. *Rock Mech. Rock Eng.* 41 (2), 267–297. doi:10.1007/s00603-007-0144-9
- Feng, Q., and Röshoff, K. (2015). "A survey of 3D laser scanning techniques for application to rock mechanics and rock engineering," in *The ISRM suggested methods for rock characterization, testing and monitoring:* 2007-2014. Cham: Springer International Publishing. 265–293.
- Grasselli, G. (2006). Manuel Rocha medal recipient shear strength of rock joints based on quantified surface description. *Rock Mech. Rock Eng.* 39 (4), 295–314. doi:10.1007/s00603-006-0100-0
- Grasselli, G., and Egger, P. (2003). Constitutive law for the shear strength of rock joints based on three-dimensional surface parameters. *Int. J. Rock Mech. Min. Sci.* 40 (1), 25–40. doi:10.1016/s1365-1609(02)00101-6
- Hu, Q., Zhao, H., Su, D., Liu, Y., and Chen, X. (2024). A simplified theoretical model to predict the shear behavior of concrete/rock joints with gaussian irregularities. $G\acute{e}otechnique$, 1–57. doi:10.1680/jgeot.24.01035
- Hudson, J. A., and Harrison, J. P. (1997). "7 Discontinuities," in Engineering rock mechanics. Oxford: Pergamon, 113-139.
- Hutson, R., and Dowding, C. (1987). Computer controlled cutting of multiple identical joints in real rock. *Rock Mech. Rock Eng.* 20, 39–55. doi:10.1007/bf01019510
- ISRM (1978). International society for rock mechanics commission on standardization of laboratory and field tests: suggested methods for the quantitative description of discontinuities in rock masses. *Int. J. Rock Mech. and Min. Sci. and Geomechanics Abstr.* 15 (6), 319–368. doi:10.1016/0148-9062(78)91472-9
- Jiang, Q., Yang, B., Yan, F., Liu, C., Shi, Y., and Li, L. (2020). New method for characterizing the shear damage of natural rock joint based on 3D engraving and 3D scanning. *Int. J. Geomechanics* 20 (2), 06019022. doi:10.1061/(asce)gm.1943-5622.0001575

- Lam, T., and Johnston, I. (1989). Shear behavior of regular triangular concrete/rock joints evaluation. *J. Geotechnical Eng.* 115 (5), 728–740. doi:10.1061/(asce)0733-9410(1989)115:5(728)
- Li, Y., Xu, Q., and Aydin, A. (2017). Uncertainties in estimating the roughness coefficient of rock fracture surfaces. *Bull. Eng. Geol. Environ.* 76 (3), 1153–1165. doi:10.1007/s10064-016-0994-z
- Li, Y., Song, L., Jiang, Q., Yang, C., Liu, C., and Yang, B. (2018). Shearing performance of natural matched joints with different wall strengths under direct shearing tests. *Geotechnical Test. J.* 41 (2), 371–389. doi:10.1520/gtj20160315
- Li, Y., Tang, C., Li, D., and Wu, C. (2020). A new shear strength criterion of three-dimensional rock joints. *Rock Mech. Rock Eng.* 53 (3), 1477–1483. doi:10.1007/s00603-019-01976-5
- Liu, Q., Tian, Y., Liu, D., and Jiang, Y. (2017). Updates to JRC-JCS model for estimating the peak shear strength of rock joints based on quantified surface description. *Eng. Geol.* 228, 282–300. doi:10.1016/j.enggeo.2017.08.020
- Liu, Q., Tian, Y., Ji, P., and Ma, H. (2018). Experimental investigation of the peak shear strength criterion based on three-dimensional surface description. *Rock Mech. Rock Eng.* 51 (3), 1005–1025. doi:10.1007/s00603-017-1390-0
- Liu, X., Zhu, W., Yu, Q., Chen, S., and Guan, K. (2019). Estimating the joint roughness coefficient of rock joints from translational overlapping statistical parameters. *Rock Mech. Rock Eng.* 52 (6), 753–769. doi:10.1007/s00603-018-1643-6
- Ma, H., Tian, Y., Liu, Q., and Pan, Y. (2020). Experimental study on the influence of height and dip angle of asperity on the mechanical properties of rock joints. *Bull. Eng. Geol. Environ.* 80 (1), 443–471. doi:10.1007/s10064-020-01904-w
- Magsipoc, E., Zhao, Q., and Grasselli, G. (2019). 2D and 3D roughness characterization. *Rock Mech. Rock Eng.* 53 (3), 1495–1519. doi:10.1007/s00603-019-01977-4
- Muralha, J., Grasselli, G., Tatone, B., Blümel, M., Chryssanthakis, P., and Yujing, J. (2014). ISRM suggested method for laboratory determination of the shear strength of rock joints: revised version. *Revis. Version. Rock Mech. and Rock Eng.* 47 (1), 291–302. doi:10.1007/s00603-013-0519-z
- Park, J.-W., and Song, J.-J. (2013). Numerical method for the determination of contact areas of a rock joint under normal and shear loads. *Int. J. Rock Mech. Min. Sci.* 58 (5), 8–22. doi:10.1016/j.ijrmms.2012.10.001
- Patton, F. D. (1966). Multiple modes of shear failure in rock. *Proc.cong.isrm Lisbon* 282, 509–513.
- Ríos-Bayona, F., Johansson, F., and Mas-Ivars, D. (2021). Prediction of peak shear strength of natural, unfilled rock joints accounting for matedness based on measured aperture. *Rock Mech. Rock Eng.* 54 (3), 1533–1550. doi:10.1007/s00603-020-02340-8
- Singh, H., and Basu, A. (2016). Shear behaviors of 'real' natural un-matching joints of granite with equivalent joint roughness coefficients. *Eng. Geol.* 211, 120–134. doi:10.1016/j.enggeo.2016.07.004
- Singh, H., and Basu, A. (2017). Evaluation of existing criteria in estimating shear strength of natural rock discontinuities. *Eng. Geol.* 232, 171–181. doi:10.1016/j.enggeo.2017.11.023
- Song, Y., Liu, B., and Liu, H. (2020). Orthogonal test method for determination of the proportion of rock-like material based on properties of deformation and brittleness. *Yantu Lixue/Rock Soil Mech.* 41 (8), 2675–2684. doi:10.16285/j.rsm.2019.1711
- Song, Y., Liu, B., and Ren, D. (2021). Study on stochastic method for the modeling of rough joints based on fractal theory. *Yanshilixue Yu Gongcheng Xuebao/Chinese J. Rock Mech. Eng.* 40 (1), 101–112. doi:10.13722/j.cnki.jrme.2020.0487
- Tang, Z. C., Jiao, Y. Y., Wong, L. N. Y., and Wang, X. C. (2016). Choosing appropriate parameters for developing empirical shear strength criterion of rock joint: review and new insights. *Rock Mech. Rock Eng.* 49 (11), 4479–4490. doi:10.1007/s00603-016-1014-0
- Tang, Z. C., Zhang, Z. F., and Jiao, Y. Y. (2021). Three-dimensional criterion for predicting peak shear strength of matched discontinuities with different joint wall strengths. *Rock Mech. Rock Eng.* 54 (6), 3291–3307. doi:10.1007/s00603-021-02471-6
- Tatone, B., and Grasselli, G. (2009). A method to evaluate the three-dimensional roughness of fracture surfaces in brittle geomaterials. *Rev. Sci. Instrum.* 80 (12), 125110. doi:10.1063/1.3266964
- Tatone, B., and Grasselli, G. (2014). An investigation of discontinuity roughness scale dependency using high-resolution surface measurements. *Rock Mech. Rock Eng.* 46 (4), 657–681. doi:10.1007/s00603-012-0294-2
- Tian, Y., Liu, Q., Liu, D., Kang, Y., Deng, P., and He, F. (2018). Updates to grasselli's peak shear strength model. *Rock Mech. Rock Eng.* 51 (7), 2115–2133. doi:10.1007/s00603-018-1469-2
- Tian, Y., Liu, H., Liu, Q., Tang, Z., Liu, Y., Zhang, J., et al. (2024). Scale effect of rock discontinuity considering all morphological information. *Geomechanics Geophys. Geo-Energy Geo-Resources* 10, 124. doi:10.1007/s40948-024-00839-w

Tian, Y., Wang, Y., Liu, Q., Tang, Z., Liu, B., Pan, Y., et al. (2025). Assessment method of surface morphology based on 100 shear tests and PSO-RBF neural network. *Rock Mech. Rock Eng.*, 1–37. doi:10.1007/s00603-025-04566-w

Tse, R., and Cruden, D. (1979). Estimating joint roughness coefficients. *Int. J. Rock Mech. Min. Sci. and Geomechanics Abstr.* 16 (5), 303–307. doi:10.1016/0148-9062(79)90241-9

Xia, C.-C., Tang, Z. C., Xiao, W. M., and Song, Y. L. (2014). New peak shear strength criterion of rock joints based on quantified surface description. *Rock Mech. Rock Eng.* 47 (2), 387–400. doi:10.1007/s00603-013-0395-6

Xie, H., Wang, J. a., and Stein, E. (1998). Direct fractal measurement and multifractal properties of fracture surfaces. *Phys. Lett. A* 242, 41–50. doi:10.1016/s0375-9601(98)00098-x

Yang, J., Rong, G., Hou, D., Peng, J., and Zhou, C. (2015). Experimental study on peak shear strength criterion for rock joints. *Rock Mech. Rock Eng.* 49 (3), 821–835. doi:10.1007/s00603-015-0791-1

Zheng, B., Qi, S., Huang, X., Guo, S., Wang, C., Zhan, Z., et al. (2020). An advanced shear strength criterion for rock discontinuities considering size and low shear rate. Appl. Sci. 10 (12), 4095. doi:10.3390/app10124095

Glossary		μ	Average value of the Gaussian distribution (°)
DEM	Digital algoriton model	σ	Standard deviation of the Gaussian distribution (°)
JRC ^{3D}	Digital elevation model Joint Roughness Coefficient (-)	$\boldsymbol{\theta}_{\scriptscriptstyle +}^*$	Apparent dip angle with $\boldsymbol{\theta}^{'}\text{>}0^{\circ}$ in the shear direction (^)
,	Two/three-dimensional	A_0	Maximum normalized contact area calculated for $\boldsymbol{\theta}_{+}^{*}\left(\%\right)$
θ^*		$A_{ m shear}$	Total area of $ heta_+^*$ (mm 2)
	Apparent dip angle (˚) Maximum apparent dip angle (˚)	\boldsymbol{A}	Total area of the rough joint surface (mm²)
θ^*_{\max}	A distribution parameter of θ^{+} proposed by Grasselli (-)	$\sigma_{ m t}$	Tensile strength of the intact rock (MPa)
C JCS	Joint wall compressive strength (MPa)	β	Angle between the normal direction of the joint and the
n	Number of iterations in "diamond-square" algorithm (-)	$A_{ heta^*}$	schistosity plane (°) Normalized area with apparent dip angles exceed $ heta^*$
m	Number of coordinate points at x-/z-coordinates (-)	l	Sampling interval in calculation of apparent dip angle in Tatone's
y	Elevation of each point on the joint surface (mm)	•	equation (mm)
Δ	Element size of DEMs (mm)	$oldsymbol{ heta_{ ext{max-eq}}^*}$	Equivalent maximum apparent dip angle ()
rand	Random parameter governing 3D morphological features of the	$F\!\left(heta_{\scriptscriptstyle+}^{st} ight)$	Complementary cumulative distribution function of $\boldsymbol{\theta}_{\scriptscriptstyle +}^*$
	fractal surfaces in "diamond-square" algorithm (mm)	$g(heta_{\scriptscriptstyle +}^*)$	Probability density function of $ heta_+^*$
d	Stochastic parameter representing the standard deviation of	$E(heta_+^*)$	Expectation of θ_+^* () (independent variable is θ_+^*)
	Gaussian distribution in "diamond-square" algorithm (mm)	$(E(\theta^* \theta^*>0^\circ))$	Conditional expectation of $\theta^* > 0^{\circ}()$ (independent variable is θ^*)
SLA	Stereolithography appearance technology applied for 3D printing	$oldsymbol{ heta}^{*'}$	Standard value of θ^* that follows the standard Gaussian distribution (-)
ISRM	International society for rock mechanics and rock engineering	$g(heta^{*})$	Probability density function of $\theta^{"}$
$ ho_0$	Natural density (g·cm ⁻³)	Φ()	Cumulative distribution function of Gaussian distribution
$\sigma_{ m c}$	Uniaxial compressive strength (MPa)	P()	Probability (-)
$\sigma_{ m t}$	Tensile strength (MPa)		Peak shear strength calculated by $E(\theta^* \theta^*>0)$ (MPa)
E	Tangential modulus at 50% uniaxial compressive strength (GPa)	$ au_{ ext{p-calculated}}$	reak siteal strength calculated by $E(b \mid b \mid b)$ (1911 a)
ν	Poisson's ratio (-)		
c	Cohesion (MPa)		
φ	Internal friction angle (˚)		
$arphi_{ m b}$	Basic friction angle (˚)		
h_i	Height of the <i>i</i> th point on joint profile (mm)		
\mathbb{Z}_2	Root mean square (-)		
s	Shear vector (-)		
CNL	Constant normal load shear condition		
$\sigma_{ m n}$	Normal stress (MPa)		
u	Shear displacement (mm)		
τ	Shear stress (MPa)		
$ au_{ m p}$	Peak shear strength (MPa)		
$ au_{ m r}$	Residual shear strength (MPa)		
JCS	Joint wall compressive strength (MPa)		
η	Shear plane		
ξ	Plane perpendicular to the triangle element		
n	Outward normal vector of the triangle element		
n_1	Component of n that parallel to the shear plane		
n_2	Component of n that perpendicular to the shear plane		
θ	Dip angle (°)		

Azimuth angle measured clockwise from $\textbf{\textit{n}}_1$ to $\textbf{\textit{s}}$ (°)